Ruthenium π-Complexes of *o*-Benzoquinone†

D. Scott Bohle,*,‡ Keith T. Carron,‡ A. Nørlund Christensen,§ Patricia A. Goodson,‡ and Anne K. Powell∥

Department of Chemistry, University of Wyoming, Laramie, Wyoming 82071-3838, Chemistry Department, Aarhus University, Langelandsgade 140, Aarhus C, Denmark, and School of Chemical Sciences, East Anglia University, Norwich NR4 7TJ, United Kingdom

Received October 6, 1993⊗

The oxidative addition of catechol to triruthenium dodecacarbonyl results in either tetranuclear ($[Ru_2(\eta^2{:}\eta^6\text{-}\mu_2\text{-}O_2C_6H_4)(CO)_4]_2$, **1a**) or hexanuclear ($[Ru_3(\eta^2{:}\eta^4\text{-}\mu_2\text{-}O_2C_6H_4)(CO)_8]_2$, **2**) complexes which contain π-bound *o*-benzoquinone ligands. Lewis bases readily add to these complexes to give either the mononuclear complexes $Ru(\eta^2\text{-}O_2C_6H_3R)(CO)_2\{EPh_3\}_2$ (**3a–d**: R = H, Me; E = P, As) and $Ru(O_2C_6H_4)(CO)_n(py)_{3-n}$ (**8** (n = 2), **9** (n = 1)), or η^4-π-complexes such as $[Ru_2(\eta^2{:}\eta^4\text{-}\mu_2\text{-}O_2C_6H_4)(CO)_4\{EPh_3\}]_2$ (**4a,b**: E = As, Sb). Mild oxidants such as iodine also oxidatively add to the Ru–Ru bond in **1a** to give the dinuclear complex $Ru_2(\mu_2\text{-}I)(\eta^2{:}\eta^4\text{-}\mu_2\text{-}O_2C_6H_4)(CO)_4I$ (**5**), where the ruthenium atoms are bridged by both iodide and quinone ligands. New complexes have been characterized by elemental analyses, IR, Raman, and ^1H and ^{13}C NMR spectroscopy, and electrochemistry. X-ray crystallographic results for four of these compounds are presented, with important unit cell data being as follows: **1a**, $Ru_4C_{20}H_8O_{12}$, crystallizes in the triclinic space group $P\bar{1}$, Z = 1, a = 6.585(2) Å, b = 8.813(2) Å, c = 10.416(2) Å, α = 99.31(3)°, β = 105.65(3)°, γ = 108.92(3)°; **3a**, $RuC_{44}H_{34}O_4P_2$, crystallizes in the orthorhombic space group *Pbcn*, Z = 4, a = 19.694(3) Å, b = 10.770(2) Å, c = 17.348(2) Å; **4a**, $Ru_4C_{56}H_{38}As_2O_{12}$, also crystallizes in the orthorhombic space group *Pbcn*, Z = 4, a = 16.412(3) Å, b = 20.624(3) Å, c = 15.483(3) Å; **5**, $Ru_2C_{10}H_4I_2O_6 \cdot {}^1/_2CH_2Cl_2$, crystallizes with two independent molecules per unit cell in the triclinic space group $P\bar{1}$, Z = 4, a = 10.222(2) Å, b = 12.418(2) Å, c = 14.621(2) Å, α = 107.97(1)°, β = 102.59(1)°, and γ = 93.87(1)°.

Although numerous studies have described ligand exchange and metal-framework-expansion reactions for metallocarbonyl clusters, our knowledge of their oxidative-addition reactions remains limited, with most examples stemming from the chemistry of triosmium dodecacarbonyl.[1,2] Surprisingly little of this chemistry has been extended to ruthenium dodecacarbonyl, even though some of the known low-valent ruthenium products from these reactions are useful catalysts and precatalysts for, among other reactions, hydroformylation and the addition of carboxylic acids to alkynes.[3] In part, this trend in observed reactivity is due to the relative strengths of the metal–metal framework bonds; while the osmium clusters often retain these bonds in the products, the iron and ruthenium clusters readily fragment.

Earlier studies have demonstrated that alcohols and phenols oxidatively add to metal–metal bonds in $Ru_3(CO)_{12}$ and $Os_3(CO)_{12}$. Aliphatic alcohols add across a single metal–metal bond to give either $M_3(\mu_2\text{-}H)(\mu_2\text{-}OR)(CO)_8$ or $M_3(\mu_2\text{-}OR)_2(CO)_8$, depending upon the metal and the conditions employed.[4] The initial products from the addition of phenols to this framework are probably similar, although the final isolated products result from a subsequent *ortho*-metalation reaction to give the C_6H_4O ligand bound as either a μ_2-C, μ_2-O fragment in the case of osmium or μ_2-C, μ_2-O, η^6-ring fragment in the case of ruthenium.[5] Hieber's pioneering work described the slow disproportionation of $Fe_3(CO)_{12}$ with methanol at room temperature to give $Fe(OCH_3)_2$, $Fe_3H_2(CO)_{11}$, and $Fe(CO)_5$. Ethanol leads to further degradation of $[Fe_3(CO)_{11}]^{2-}$ to $[Fe(CO)_4]^{2-}$.[6] Alkoxide-bridged structures similar to those found for osmium and ruthenium trimetallododecacarbonyls are likely, albeit undetected, intermediates in these reactions.

In the course of our studies of the oxidative-addition reactions of simple oxo species such as carboxylic acids,[7] phosphinic acids,[7,8] aldehydes,[9] and formyl ylides[2,10] to triruthenium dodecacarbonyl, we examined the unreported

† Dedicated to Professor Herbert D. Kaesz on the occasion of his 60th birthday.

‡ University of Wyoming.

§ Aarhus University.

∥ East Anglia University.

⊗ Abstract published in *Advance ACS Abstracts,* March 1, 1994.

(1) Shriver, D. F.; Kaesz, H. D.; Adams, R. D. *The Chemistry of Metal Cluster Complexes*; VCH: Weinheim, Germany, 1990.

(2) Heineke, D.; Bohle, D. S.; Vahrenkamp, H. *Chem. Ber.* **1993,** *126,* 355.

(3) (a) Jenck, J.; Kalck, P.; Pinelli, E.; Siani, M.; Thorez, A. *J. Chem. Soc., Chem. Commun.* **1988,** 1428. (b) Rotem, M.; Shvo, Y. *Organometallics* **1983,** *2,* 1689.

(4) (a) Johnson, B. F. G.; Lewis, J.; Kilty, P. A. *Chem. Commun.* **1968,** 180. (b) Johnson, B. F. G.; Lewis, J.; Kilty, P. A. *J. Chem. Soc. A* **1968,** 2859. (c) Azam, K. A.; Deeming, A. J.; Kimber, R. E.; Shukla, P. R. *J. Chem. Soc., Dalton Trans.* **1976,** 1853. (d) Azam, K. A.; Deeming, A. J.; Rothwell, I. P.; Hursthouse, M. B.; New, L. *J. Chem. Soc., Chem. Commun.* **1978,** 1086. (e) Bryan, E. G.; Johnson, B. F. G., Lewis, J. *J. Chem. Soc., Dalton Trans.* **1977,** 1328. Crooks, G. R.; Johnson, B. F. G.; Lewis, J. *J. Chem. Soc. A* **1969,** 797. (f) Aime, S.; Botta, R.; Gobetto, R.; Osella, D.; Padovan, F. *J. Chem. Soc., Dalton Trans.* **1987,** 253. (g) Santini, C. C.; Basset, J.-M.; Fontal, B.; Krause, J.; Shore, S.; Charrier, C. *J. Chem. Soc., Chem. Commun.* **1987,** 512. (h) Van Doorn, J. A.; Van Leeuwen, P. W. N. M. *J. Organomet. Chem.* **1981,** *222,* 299.

(5) Bohle, D. S.; Vahrenkamp, H. *Angew. Chem., Int. Ed. Engl.* **1990,** *29,* 198.

(6) (a) Hieber, W.; Vetter, H. *Chem. Ber.* **1931,** *64,* 2340. (b) Hieber, W.; Brendel, G. *Z. Anorg. Allg. Chem.* **1957,** *289,* 338. (c) Hieber, W. *Angew. Chem.* **1960,** *72,* 795. (d) Hieber, W.; Schubert, E. H. *Z. Anorg. Allg. Chem.* **1965,** *338,* 37.

(7) Bohle, D. S.; Vahrenkamp, H. *Inorg. Chem.* **1990,** *29,* 1097.

(8) Barnes, C. A.; Bohle, D. S. Unpublished results.

(9) Bohle, D. S.; Breidt, V. F.; Powell, A. K.; Vahrenkamp, H. *Chem. Ber.* **1992,** *125,* 1111.

(10) Bohle, D. S.; Heineke, D.; Tiripicchio, A.; Tiripicchio-Camellini, M.; Vahrenkamp, H. *Angew. Chem., Int. Ed. Engl.* **1990,** *29,* 896.

0276-7333/94/2313-1355$04.50/0

reaction of catechol with this cluster.[11] Our initial results indicated that in addition to the expected η^2-O-bound chelate binding of catechol to the metal fragment, the catechol was also bound in a very unusual η^n-π-manner that was without precedent in the extensive literature concerning ruthenium catecholate complexes.[12] The compelling question behind most of this prior research has concerned the factors which determine the localization of electrons between the ruthenium and quinone fragment as in the valence tautomers **A**–**C**.[13] Elegant recent studies

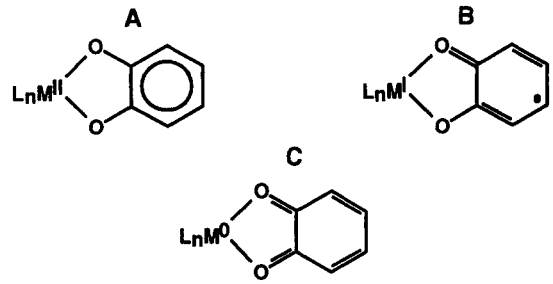

by Hendrickson *et al.* and Pierpont *et al.* demonstrates that for first-row transition metals a temperature-dependent bistability exists for these valence tautomers; *cf.* in [Co(phen)(3,5-dtbsq)(3,5-dtbq)] there is a transition from an $S = {}^1/_2$Co(III) species to a higher spin Co(II) complex at 250 K.[14ab] Therefore, a particularly important problem we sought to address in our research was how π-bonding of the quinone to a second metal modifies the electronic structure and the valence tautomerism in **A**–**C**.

Quinonoid cofactors are important in many electron-transfer processes, and in this regard their role in photosystem II has been intensively studied. In addition, many enzymes also require the presence of quinonoid cofactors to assist in electron transfer from the surface of the protein to the active site. The last 7 years have seen the recognition of yet a third broad category of biologically relevant quinonoid species, the quinoproteins, where the quinone is located at the active site and is prepared by the oxidative modification of the amino acid side chains already present at the site.[15] Examples of these enzymes include galactose oxidase and the amine oxidases, which contain tyrosyl(4-thioether)[16] and topaquinone[18] residues, respectively. The metal–quinonoid cofactor π-interaction may be rather common[15a] and critical to enzymatic turnover.[19] In the context of this report it is important to note that several of these enzymes contain metals in close proximity to the quinone cofactor and that the resulting ensemble can act as a two-electron center. In this case the strength of the metal–quinone can be expected to alter the redox potential of this ensemble, probably to a degree intermediate between the extreme represented by the complexes described in this report and that corresponding to independent noninteracting centers. Thus, just as constellations of metal atoms can act in a concerted manner to affect multielectron redox changes,[20] a constellation or juxtaposition of metal and quinonoid cofactors can possibly achieve similar results.

This paper details (a) the synthesis of two ruthenium carbonyl π-bound quinone adducts by direct oxidative addition of catechol to triruthenium dodecacarbonyl, (b) the structures of these new π-quinone complexes, which include an unusual example of a π-stacked metalloquinone chain, and (c) reactions of these unusual π-complexes. Some of these results have been communicated before.[21]

Results and Discussion

The syntheses of the starting materials $[Ru_2(\eta^2{:}\eta^6\text{-}\mu_2\text{-}O_2C_6H_4)(CO)_4]_2$ (**1a**) and $[Ru_3(\eta^2{:}\eta^4\text{-}\mu_2\text{-}O_2C_6H_4)(CO)_8]_2$ (**2**) are outlined in eqs 1 and 2. These preparations utilize

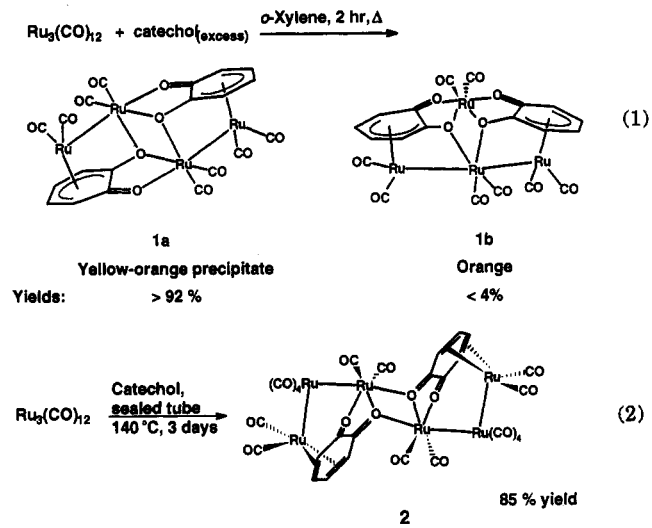

large excesses of catechol, which are easily separated from the crystalline products by either filtration, in the case of **1a**, or sublimation, in the preparation of **2**. The tetranuclear complex **1a** is completely insoluble in all solvents with the exception of coordinating solvents such as tetrahydrofuran and acetonitrile at reflux, with which it reacts. If lower catechol to $Ru_3(CO)_{12}$ ratios are used for the preparation of **1a** (*e.g.* 1:3, where only a 2-fold excess of catechol is used), the yield of **1a** is reduced to *ca.* 55%. Although most of the byproducts from these syntheses are insoluble dark solids, the isomeric product $[Ru_4(CO)_8(\eta^2{:}\eta^5\text{-}\mu_2\text{-}O_2C_6H_4)_2]$ (**1b**), which forms in low yields (<4%), was identified by spectroscopy and by comparison to recently reported values for the structurally characterized

(11) The reactions of oxo acids with triosmium dodecacarbonyl have recently been reviewed: Frauenhoff, G. R. *Coord. Chem. Rev.* **1992**, *121*, 131.

(12) For recent references concerning ruthenium catecholate compounds, see: (a) Masui, H.; Lever, A. B. P.; Dodsworth, E. S. *Inorg. Chem.* **1993**, *32*, 258. (b) Lever, A. B. P.; Masui, H.; Metcalfe, R. A.; Stufkens, D. J.; Dodsworth, E. S.; Auburn, P. R. *Coord. Chem. Rev.* **1993**, *125*, 317. (c) Boone, S. R.; Pierpont, C.G. *Polyhedron* **1990**, *9*, 2267.

(13) Pierpont, C. G.; Buchanan, R. M. *Coord. Chem. Rev.* **1981**, *38*, 45.

(14) (a) Adams, D. M.; Dei, A.; Rheingold, A. L.; Hendrickson, D. N. *Angew. Chem., Int. Ed. Engl.* **1993**, *32*, 880. (b) Pierpont, C. G. Private communication.

(15) For reviews of quinoproteins, see: (a) Duine, J. A. *Eur. J. Biochem.* **1991**, *200*, 271. (b) Jonegejan, J. A.; Duine, J. A., Eds. *PQQ and Quinoproteins*; Kluwer: Dordrecht, The Netherlands, 1989. (c) Thompson, A. J. *Nature* **1991**, *350*, 22.

(16) Derived from the covalent linkage of the cysteinyl sulfur in cys 228 to the 4-position of the phenyl ring in tyr 272.[17]

(17) Ito, N.; Phillips, S. E. V.; Stevens, C.; Ogel, Z. B.; McPherson, M. J.; Keen, J. N.; Yadav, D. S.; Knowles, P. F. *Nature* **1991**, *350*, 87.

(18) Topaquinone = 3-(2,4,5-trihydroxyphenyl)alanine; see: James, S. M.; Mu, D.; Wemmer, D.; Smith, A. J.; Kaur, S.; Maltby, D.; Burlingame, A. L.; Klinman, J. P. *Science* **1991**, *248*, 981.

(19) (a) Dooley, D. M.; McGuirl, M. A.; Brown, D. E.; Turowski, P. N.; McIntire, W. S.; Knowles, P. F. *Nature* **1991**, *349*, 262. (b) Nakamura, N.; Kohzuma, T.; Kuma, H.; Suzuki, S. *J. Am. Chem. Soc.* **1992**, *114*, 6550. (c) Branchaud, B. P.; Montague-Smith, M. P.; Kosman, D. J.; McLaren, F. R. *J. Am. Chem. Soc.* **1993**, *115*, 798.

(20) For an example of the dynamics of multicopper constellations in enzymes, see: Solomon, E. I.; Lowery, M. D. *Science* **1993**, *259*, 1575.

(21) (a) Bohle, D. S.; Goodson, P. A. *J. Chem. Soc., Chem. Commun.* **1992**, 1205. (b) Bohle, D. S.; Christensen, A. N.; Goodson, P. A. *Inorg. Chem.* **1993**, *32*, 4173.

Table 1. Infrared Data for New Compounds[a]

compd	compd no.	ν(C–O)[b]	other bands
$[Ru_2(\mu_2\text{-}\eta^2\text{:}\eta^6\text{-}O_2C_6H_4)(CO)_4]_2$	**1a**	2053, 2006.2, 1964.3, 1954.6	1518.8 m, 1463.8 s, 1420.4 m, 1336 s, 1322 s, 1252.1 m
$[Ru_2(\mu_2\text{-}\eta^2\text{:}\eta^6\text{-}O_2C_6H_4)(CO)_4]$[c]	**1b**	2064 w, 2036 vs, 2000 m, 1990 w, 1958 m br	
$[Ru_3(\mu_2,\mu_2\text{-}\eta^2\text{:}\eta^4\text{-}O_2C_6H_4)(CO)_8]_2$	**2**	2084, 2036.5, 2013.1, 1979.2, 1953.1, 1927.1	1512 m, 1461.1 s, 1419.4 w, 1375 w, 1317.7 w, 1299.1 m, 1267 s
$Ru(\eta^2\text{-}O_2C_6H_4)(CO)_2(PPh_3)_2$	**3a**	2029.1, 1966.4, 1937.7 sh, 1904 w, 1888.1 w	1475.9 s,[c] 1435.4 m,[c] 1257.9 s (ν(C–O)$_{catechol}$)
$Ru(\eta^2\text{-}O_2C_6H_4)(CO)_2(AsPh_3)_2$	**3b**	2027.9, 1965.7	1475.4 s,[c] 1436.3 m,[c] 1256 s (ν(C–O)$_{catechol}$)
$Ru\{\eta^2\text{-}O_2C_6H_3(4\text{-}Me)\}(CO)_2(PPh_3)_2$	**3c**	2031.3, 1961.9	1487.9 s, 1433.4 m, 1271.4 s, 1256.5 s
$Ru\{\eta^2\text{-}O_2C_6H_3(4\text{-}Me)\}(CO)_2(AsPh_3)_2$	**3d**	2027.4, 1960.4	1484.0 s, 1435.4 m, 1270.0 s, 1254.5 s
$[Ru_2(\mu_2\text{-}\eta^2\text{:}\eta^4\text{-}O_2C_6H_4)(CO)_4(AsPh_3)]_2$	**4a**	2049.1 w, 2024.5, 2007.2, 1979.1, 1965.2 w, 1927.6, 1920.9, 1904 w	1496.1 s,[c] 1434.4 m, 1351 m, 1333.6 s, 1304.7 w
$[Ru_2(\mu_2\text{-}\eta^2\text{:}\eta^4\text{-}O_2C_6H_4)(CO)_4(SbPh_3)]_2$	**4b**	2023.6, 2006.7, 1980.7, 1967.2 w, 1928.6, 1923.2, 1904.5 w	1493.2 s, 1432.5 m, 1348.1 m, 1332.2 m, 1301.3 w
$Ru_2(\mu_2\text{-}\eta^2\text{:}\eta^4\text{-}O_2C_6H_4)(CO)_4(\mu_2\text{-}I)(I)$	**5**	2088.6 w, 2079.7 m, 2055.6, 2024.5, 1991.4, 1967.1 w	1505.2 s (ν(C–O)$_{catechol}$), 1475.3 m, 1467.4 m, 1429.8 w, 1376.7 w, 1354.1 w, 1329.2 w
$Ru_2(\mu_2\text{-}\eta^2\text{:}\eta^4\text{-}O_2C_6H_4)(CO)_4(I)_2(py)$	**6**	2053.9, 2000 sh, 1993.2	1536.6 m (ν(C–O)$_{catechol}$), 1518.3 m, 1482.6 m, 1354.8 w, 1330.7 w
$RuI_2(CO)_2(py)_2$	**7**	2049.1, 1988.4	1604.1 w, 1484 w, 1443.1 m, 1211.6 w, 1067.5 m, 761.8 m, 699.6 m
$Ru(\eta^2\text{-}O_2C_6H_4)(CO)_2(py)_2$	**8**	2034.2, 1962	1476.8 s, 1450.8 m, 1259.8 s
$Ru(\eta^2\text{-}O_2C_6H_4)(CO)(py)_3$	**9**	1903.5	1474.9 s, 1447.4 m, 1258.4 s

[a] In cm^{-1}. Spectra were recorded as KBr pellets unless noted. Bands due to EPh_3 (E = P, As, Sb) ligands are not included. [b] All carbonyl bands are strong unless indicated otherwise: s = strong, m = medium, w = weak, sh = shoulder. [c] Overlap of ν(C–O)$_{catechol}$ bands and bands due to EPh_3 ligands preclude definitive assignment.

complex.[22] Solvents such as benzene and toluene can also be employed in the reaction, although there is an increase in the required reaction times (36 h for benzene) and a slightly reduced yield of product **1a**. Significantly absent from these reactions are the μ_6-carbido products $Ru_6(\mu_6\text{-}C)(CO)_{18}(\eta^6\text{-}C_6Me_nH_{6-n})$ (n = 0, 1, 3), which are known to result from the thermal fragmentation of $Ru_3(CO)_{12}$ in these solvents,[23] and hydride-containing products $Ru_4H_4(CO)_{12}$ and $Ru_4H_2(CO)_{13}$. This latter result is also found for the products of the oxidative addition of carboxylic and phosphinic acids to triruthenium dodecacarbonyl, which also undergo a formal double oxidative addition.[7,8,24] Although we have not determined or quantified the gaseous byproduct of these reactions, dihydrogen and carbon monoxide are the presumed byproducts in eqs 1 and 2. Relevant IR and NMR spectroscopic data for all new compounds are collected in Tables 1 and 2, respectively.

During the sealed-tube reaction in eq 2, triruthenium dodecacarbonyl initially dissolves into the catechol melt to give an orange-yellow solution from which there is a steady evolution of gas. This reaction results in a deep red-orange solution from which large crystals of **2** slowly crystallize. Gradual cooling followed by sublimation of the excess catechol, and traces of triruthenium dodecacarbonyl, yields analytically pure **2** as a catechol solvate. Higher temperatures, in excess of 160 °C, lead to the formation of considerable quantities of an insoluble unidentified black material. Although **2** is sufficiently soluble and stable in halocarbon solvents to allow us to measure ^{1}H and ^{13}C NMR spectra, as well as to perform electrochemical characterization, it decomposes rapidly on silica and alumina, thus precluding column chromatographic separation. As a consequence, most of the studies with **2** have employed the catechol-solvated crystals which are obtained directly from the sealed-tube preparations.

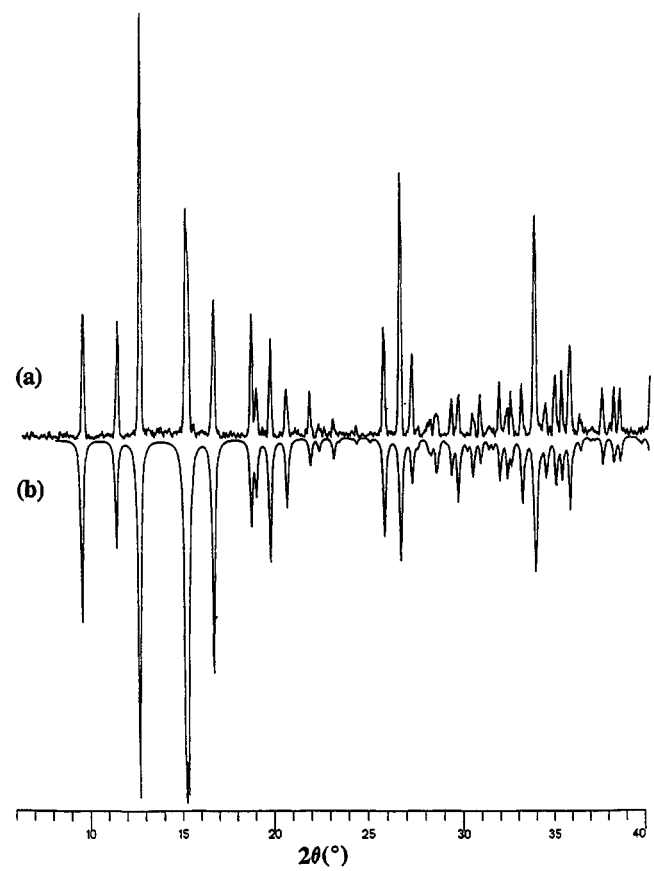

Figure 1. Observed (a) and calculated (b) powder diffraction patterns for $[Ru_2(O_2C_6H_4)(CO)_4]_2$ (**1a**) with Cu Kα_1 radiation (λ = 1.540 60 Å).

The structural characterization of **1a** has been accomplished by both powder and single-crystal X-ray diffraction techniques. The microcrystalline precipitate which results from the conditions in eq 1 gives a sharp powder diffraction pattern (Figure 1a) out to 65° in 2θ with Cu Kα_1 radiation. This pattern has been indexed and gives a triclinic unit

(22) Churchill, M. R.; Lake, C. H.; Paw, W.; Keister, J. B. *Organometallics* **1994**, *13*, 8.
(23) (a) Mason, R.; Robinson, W. R. *Chem. Commun.* **1968**, 468. (b) Johnson, B. F. G.; Johnston, R. D.; Lewis, J. *J. Chem. Soc. A* **1968**, 2865.
(24) Crooks, G. R.; Johnson, B. F. G.; Lewis, J.; Williams, I. G.; Gamlen, G. *J. Chem. Soc. A* **1969**, 2761.

Table 2. ^1H and ^{13}C NMR Data for New Compounds[a]

compound		^1H	$^{13}C\{^1H\}$
$[Ru_3(\mu_2,\mu_2\text{-}\eta^2\text{:}\eta^4\text{-}O_2C_6H_4)(CO)_8]_2$	**2**	5.84 (dd, $^3J_{HH}$ = 5.0, $^4J_{HH}$ = 3.2, 2, C*H*); 5.28 (dd, 2, C*H*)	208.7, 207.0, 198.9, 198.8, 197.9, 198.5 (s, Ru—*C*═O); 158.3, 158.2 (s, *C*—ORu); 124.9, 110.5, 88.0, 81.4 (s, *C*H)
$Ru(\eta^2\text{-}O_2C_6H_4)(CO)_2(PPh_3)_2$[b]	**3a**	7.81 (m, P(C_6H_5)$_3$, 12); 6.96 (m, P(C_6H_5)$_3$, 18); 6.44 (dd, $^3J_{HH}$ = 5.5, $^4J_{HH}$ = 3.6, 2, C*H*); 6.34 (dd, 2, C*H*)	*c*
$Ru(\eta^2\text{-}O_2C_6H_4)(CO)_2(AsPh_3)_2$	**3b**	7.32 (m, As(C_6H_5)$_3$, 30); 5.97 (dd, $^3J_{HH}$ = 5.3, $^4J_{HH}$ = 3.5, 2, C*H*); 5.87 (dd, 2, C*H*)	196.4 (s, Ru—*C*—O); 159.5 (s, *C*—ORu); 133.7, 131.8, 130.2, 128.7 (s, As(C_6H_5)$_3$); 115.2, 115.0 (s, C_4H_4)
$Ru\{\eta^2\text{-}O_2C_6H_3(4\text{-}Me)\}(CO)_2(PPh_3)_2$[b]	**3c**	6.97 (m, P(C_6H_5)$_3$, 30); 6.36 (dd, $^3J_{HH}$ = 7.8, $^4J_{HH}$ = 3.5, 1, {3-C*H*}); 6.12 (m, 1, C*H*); 6.12 (d, 1, C*H*); 2.14 (s, 3, CH_3)	*c*
$Ru\{\eta^2\text{-}O_2C_6H_3(4\text{-}Me)\}(CO)_2(AsPh_3)_2$[b]	**3d**	7.73 and 6.95 (m, As(C_6H_5)$_3$, 30); 6.83 (d, $^3J_{HH}$ = 4.9, 1, {3-C*H*}); 6.70 (d, $^3J_{HH}$ = 1.0, 1, C*H*); 6.66 (dd, 1, C*H*); 2.14 (s, 3, CH_3)	197.7 (s, Ru—*C*—O); 160.2 (s, *C*—ORu); 134.3, 132.61, 130.3, 128.5 (s, As(C_6H_5)$_3$); 123.9, 116.8, 116.3, 114.7 (s, C_4H_3); 21.24 (s, CH_3)
$[Ru_2(\mu_2\text{-}\eta^2\text{:}\eta^4\text{-}O_2C_6H_4)(CO)_4(AsPh_3)]_2$	**4a**	7.38 (m, As(C_6H_5)$_3$, 15); 5.79 (dd, $^3J_{HH}$ = 6.8, $^4J_{HH}$ = 1.8, 1, C*H*); 5.57 (dd, $^3J_{HH}$ = 7.0, $^4J_{HH}$ = 1.5, 1, C*H*); 5.15 (ddd, $^3J_{HH}$ = 6.6, $^4J_{HH}$ = 1.3 and 1.3, 1, C*H*); 4.84 (ddd, $^3J_{HH}$ = 6.4, $^4J_{HH}$ = 1.7 and 1.2, 1, C*H*)	203.6, 203.4, 203.1, 203.0 (s, Ru—*C*═O); 163.7, 155.8 (s, *C*—ORu); 133.0, 133.9, 130.5, 129.4 (s, As(C_6H_5)$_3$); 98.9, 87.1, 86.9, 80.0 (s, C_4H_4)
$[Ru_2(\mu_2\text{-}\eta^2\text{:}\eta^4\text{-}O_2C_6H_4)(CO)_4(SbPh_3)]_2$	**4b**	7.39 (m, Sb(C_6H_5)$_3$, 15); 5.94 (dd, $^3J_{HH}$ = 7.3, $^4J_{HH}$ = 1.7, 1, C*H*); 5.65 (dd, $^3J_{HH}$ = 6.6, $^4J_{HH}$ = 1.3, 1, C*H*); 5.14 (ddd, $^3J_{HH}$ = 7.3 and 6.3, $^4J_{HH}$ = 1.7, 1, C*H*); 4.88 (ddd, $^3J_{HH}$ = 6.6 and 6.3, $^4J_{HH}$ = 1.3, 1, C*H*)	*c*
$Ru_2(\mu_2\text{-}\eta^2\text{:}\eta^4\text{-}O_2C_6H_4)(CO)_4(\mu_2\text{-}I)(I)$	**5**	6.01 (dd, $^3J_{HH}$ = 4.9, $^4J_{HH}$ = 2.9, 2, C*H*); 5.30 (dd, 2, C*H*)	196.1, 190.8 (s, Ru—*C*—O); 165.2 (s, *C*—ORu); 85.3, 79.9 (s, C_4H_4)
$Ru_2(\mu_2\text{-}\eta^2\text{:}\eta^4\text{-}O_2C_6H_4)(CO)_4(I)_2(py)$	**6**	8.49 (dd, $^3J_{HH}$ = 6.6, $^4J_{HH}$ = 2.0, 2, NC_5H_5, CH_o); 7.89 (tt, $^3J_{HH}$ = 7.9, 1, NC_5H_5, CH_p); 7.53 (td, $^3J_{HH}$ = 6.4, 2, NC_5H_5, CH_m); 5.73 (dd, $^3J_{HH}$ = 4.6, $^4J_{HH}$ = 3.3, 2, C*H*); 5.54 (dd, 2, C*H*)	*c*
$RuI_2(CO)_2(py)_2$	**7**	9.05 (dd, $^3J_{HH}$ = 6.6, $^4J_{HH}$ = 1.3, 2, NC_5H_5, CH_o); 7.86 (tt, $^3J_{HH}$ = 7.9, 1, NC_5H_5, CH_p); 7.35 (ddd, $^3J_{HH}$ = 6.9, 2, NC_5H_5, CH_m)	196.7 (s, Ru—*C*—O); 156.3 (s, NC_5H_5, C_o); 138.5 (s, NC_5H_5, C_p); 125.1 (s, NC_5H_5, C_m)
$Ru(\eta^2\text{-}O_2C_6H_4)(CO)_2(py)_2$	**8**[b]	8.59 (dd, $^3J_{HH}$ = 6.3, $^4J_{HH}$ = 1.3, 2, NC_5H_5, CH_o); 7.29 (dd, $^3J_{HH}$ = 5.8, $^4J_{HH}$ = 3.6, 2, $C_6H_4O_2$, C*H*); 6.78 (dd, $^3J_{HH}$ = 5.6, $^4J_{HH}$ = 3.4, 2, $C_6H_4O_2$, C*H*); 6.37 (tt, $^3J_{HH}$ = 7.7, 1, NC_5H_5, CH_p); 6.06 (t, $^3J_{HH}$ = 7.1, 2, NC_5H_5, CH_m)	*c*
$Ru(\eta^2\text{-}O_2C_6H_4)(CO)(py)_3$	**9**[b]	8.90 (d, $^3J_{HH}$ = 5.1, 2, NC_5H_5, CH_o); 8.56 (d, $^3J_{HH}$ = 6.4, 4, NC_5H_5, CH_o); 7.53 (dd, $^3J_{HH}$ = 6.6, $^4J_{HH}$ = 2.3, 1, $C_6H_4O_2$, C*H*); 7.42 (dd, $^3J_{HH}$ = 6.8, $^4J_{HH}$ = 2.1, 1, $C_6H_4O_2$, C*H*); 6.89 (m, 2, $C_6H_4O_2$, C*H*); 6.54 (t, $^3J_{HH}$ = 7.7, 1, NC_5H_5, CH_p); 6.45 (t, $^3J_{HH}$ = 7.7, 2, NC_5H_5, CH_p); 6.21 (t, $^3J_{HH}$ = 7.1, 2, NC_5H_5, CH_m); 6.11 (t, $^3J_{HH}$ = 7.1, 4, NC_5H_5, CH_m)	*c*

[a] Except where noted, the spectra were measured in $CDCl_3$ at 22 °C. Chemical shifts are in ppm with respect to tetramethylsilane, and coupling constants are given in hertz. [b] C_6D_6 used as solvent. [c] Spectrum not measured.

cell with lattice constants a = 6.584 Å, b = 8.809 Å, c = 10.717 Å, α = 99.31°, β = 105.64°, and γ = 110.71° and a very small volume of V = 529.7 Å^3. Experimental and calculated powder diffraction peaks are collected in the supplementary material. The density of the crystallites as determined by flotation techniques is 2.70 (±0.05) g cm^{-3}. Therefore, the mass of the contents of the unit cell is 860 ± 15 g, which corresponds to two units of $[Ru_2(CO)_4(O_2C_6H_4)]$, the empirical formula which best conformed to the elemental analysis of **1a**. The two possible crystallographic situations compatible with these results are (1) the molecule crystallizes in the space group $P1$ with two independent units of $Ru_2(CO)_4(O_2C_6O_4)$ and (2) the two units are related by an inversion center and the compound crystallizes in the $P\bar{1}$ space group. A modified synthesis of **1a**, namely by use of reduced temperatures (127 *vs* 139 °C), longer preparation times (56 h *vs* 2 h), and higher concentrations of reactants (*ca.* 20-fold greater concentration), allowed for the isolation of **1a** as deep orange crystals suitable for single-crystal X-ray diffraction. The single-crystal X-ray diffraction result for **1a**, described below, confirmed the cell geometry obtained by powder diffraction and proved that the space group is indeed $P\bar{1}$. An ORTEP view of **1a** is shown in Figure 2. Important metrical parameters and atomic positions are collected in Tables 3 and 4, respectively. This determination allowed us to calculate the expected powder diffraction pattern, shown in Figure 1b. As can be seen by the match in the observed and calculated 2θ values, the two experiments are in excellent agreement, and all diffraction peaks in the bulk phase prepared by eq 1 are accounted for in the single-crystal experiment. The relative intensities of the calculated and observed diffraction peaks are very similar to one another and suggest that preferred orientation effects do not significantly alter the relative intensities of the diffraction peaks. Most importantly, though, these results demonstrate that both syntheses yield the same phase of **1a**, and the structure shown in Figure 2 is that of the bulk

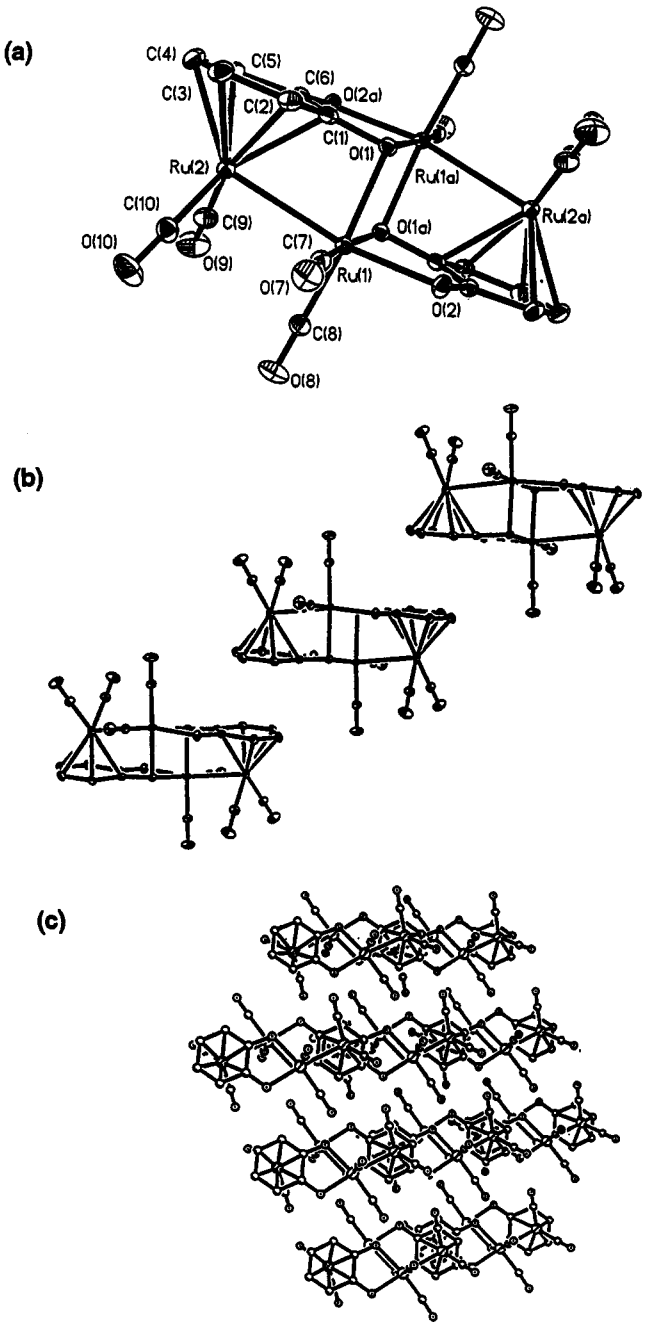

Figure 2. π-Stacking in the crystal lattice of $[Ru_2(O_2C_6H_4)(CO)_4]_2$ (**1a**). View a shows the numbering scheme for an individual molecule. View b is of a chain of π-stacked molecules which have an average intermolecular carbon–carbon bond distance of 3.596 Å. View c illustrates how these chains pack together and shows the eclipsing geometries between adjacent rings.

sample. Crystals of **2** suitable for single-crystal X-ray diffraction were grown during the sealed-tube preparation. An ORTEP view of **2** has already been published; metrical results and atomic position data are collected in the supplementary material.[21b]

The structures of **1a** and **2** illustrate the flexibility in the bonding modes for the quinone ligand. Both complexes contain quinone fragments which bridge three metals and have similar η^2-O, μ_2-O, and π-arene motifs. Furthermore, both have two π-*o*-benzoquinone ligands, which are related by crystallographically imposed inversion symmetry. In each case this inversion center is located in the parallelogram defined by the μ_2-oxygen and bridged ruthenium atoms. A significant difference in these two structures, however, is the conformation of the quinone and non-π-bound $Ru(CO)_2(\eta^2$-O) fragment. In the case of **1a**, these are coplanar; however, in **2** the two planes defined by these fragments form a dihedral angle of 149°.

Complex **2** can be viewed as an edge-bridged triruthenium cluster where η^2-O coordination on Ru(1) results in labilization of a carbon monoxide ligand and the concomitant formation of the μ_2-O bridge to a second $Ru_3(CO)_8(O_2C_6H_4)$ fragment. The structural consequences of the quinone bridging a cluster edge are a cleavage of the metal–metal bond, which lengthens the ruthenium–ruthenium distance to 4.1 Å, and a widening of the intermetal bond angle at Ru(3) to 91.8°. An alternative

Table 3. Selected Metrical Parameters for $[Ru_2(O_2C_6H_4)(CO)_4]_2$ (1a)

Bond Lengths (Å)			
Ru(1)–Ru(2)	2.775(1)	O(1)–C(1)	1.351(3)
Ru(1)–O(1)	2.192(2)	O(2)–C(6A)	1.292(3)
Ru(1)–O(2)	2.097(2)	C(7)–O(7)	1.140(4)
Ru(1)–C(7)	1.839(3)	C(8)–O(8)	1.131(4)
Ru(1)–C(8)	1.849(3)	C(9)–O(9)	1.153(6)
Ru(1)–O(1A)	2.206(2)	C(10)–O(10)	1.126(4)
Ru(2)–C(9)	1.851(4)	C(1)–C(2)	1.416(4)
Ru(2)–C(10)	1.877(3)	C(1)–C(6)	1.453(5)
Ru(2)–C(1)	2.319(3)	C(2)–C(3)	1.405(4)
Ru(2)–C(2)	2.313(4)	C(3)–C(4)	1.410(6)
Ru(2)–C(3)	2.302(4)	C(4)–C(5)	1.398(4)
Ru(2)–C(4)	2.300(3)	C(5)–C(6)	1.430(3)
Ru(2)–C(5)	2.325(3)		
Ru(2)–C(6)	2.402(3)		
Bond Angles (deg)			
Ru(2)–Ru(1)–O(1)	80.7(1)	O(2)–Ru(1)–O(1A)	79.6(1)
O(1)–Ru(1)–O(2)	88.3(1)	Ru(1)–Ru(2)–C(9)	87.9(1)
Ru(1)–Ru(2)–C(3)	114.9(1)	Ru(1)–Ru(2)–C(10)	95.5(1)
O(1)–Ru(1)–C(8)	169.6(1)	Ru(1)–Ru(2)–C(1)	62.3(1)
Ru(1)–O(1)–Ru(1A)	102.7(1)	C(1)–C(6)–O(2A)	120.7(2)
C(1)–O(1)–Ru(1A)	107.9(2)	Ru(2)–Ru(1)–O(2)	167.7(1)
O(1)–Ru(1)–O(1A)	77.3(1)	O(1)–Ru(1)–C(7)	101.2(1)
C(8)–Ru(1)–O(1A)	95.6(1)	Ru(2)–Ru(1)–C(8)	93.8(1)
Ru(2)–C(1)–O(1)	122.2(2)	O(2)–Ru(1)–C(8)	97.9(1)
O(1)–C(1)–C(2)	122.4(3)	Ru(1)–Ru(2)–C(4)	138.3(1)
Ru(2)–C(6)–O(2A)	129.7(2)	Ru(1)–O(2)–C(6A)	112.5(2)
Ru(1)–Ru(2)–C(2)	79.8(1)	C(7)–Ru(1)–O(1A)	172.7(1)
Ru(2)–Ru(1)–C(7)	83.6(1)	Ru(1)–Ru(2)–C(5)	117.8(1)
O(2)–Ru(1)–C(7)	93.2(1)	Ru(2)–C(1)–C(2)	72.0(2)
Ru(1)–O(1)–C(1)	94.5(2)	O(1)–C(1)–C(6)	118.3(2)
C(7)–Ru(1)–C(8)	86.8(1)	C(5)–C(6)–O(2A)	121.2(3)
Ru(2)–Ru(1)–O(1A)	103.1(1)		

Table 4. Atomic Coordinates (×10⁴) and Equivalent Isotropic Displacement Coefficients (Å² × 10³) for $[Ru_2(O_2C_6H_4)(CO)_4]_2$ (1a)

	x	*y*	*z*	*U*(eq)[a]
Ru(1)	1547(1)	4711(1)	6488(1)	21(1)
Ru(2)	3882(1)	8117(1)	7701(1)	24(1)
O(1)	1933(3)	5510(2)	4651(2)	23(1)
O(2)	143(3)	2234(2)	5265(2)	29(1)
C(7)	4359(5)	4640(3)	7281(3)	27(1)
O(7)	6035(4)	4491(3)	7756(3)	44(1)
C(8)	948(5)	4296(4)	8060(3)	29(1)
O(8)	560(5)	4037(4)	9015(3)	48(1)
C(9)	1633(6)	8046(4)	8467(3)	35(1)
O(9)	243(5)	8056(4)	8941(3)	59(1)
C(10)	5546(5)	7928(4)	9398(3)	33(1)
O(10)	6500(5)	7836(4)	10438(3)	55(1)
C(1)	3187(5)	7127(3)	5357(3)	24(1)
C(2)	5577(5)	7736(4)	6064(3)	30(1)
C(3)	6771(5)	9382(4)	6913(3)	34(1)
C(4)	5620(6)	10459(4)	7079(3)	36(1)
C(5)	3275(5)	9898(3)	6355(3)	31(1)
C(6)	2013(5)	8261(3)	5426(3)	25(1)

[a] Equivalent isotropic *U*, defined as one-third of the trace of the orthogonalized U_{ij} tensor.

perspective of this pair of structures is that **2** corresponds to **1a**, where there is a $Ru(CO)_4$ fragment inserted into the ruthenium–ruthenium bond.

The complex **1a** clearly contains significantly different carbon–oxygen bond lengths of 1.351(3) Å for O(1) and 1.292(3) Å for O(2). On the other hand, these values in **2**, 1.316(6) Å for O(2) and 1.306(6) Å for O(1), not only are intermediate between those for **1a** but also are not significantly different. On the basis of these trends alone **1a** is semiquinone-like, while **2** is quinone-like. The trends in metal–carbon bond distances and, more significantly, the degree of ring slippage provide an insight into the hapticity of the π-bound quinone. Ring slippage is calculated by determining the distance and direction between the vector which connects the metal to the arene ring centroid and the vector normal to the plane defined by the arene. In each structure containing π-bound quinones described in this report, the ring is slipped away from C(1) and C(6), the oxygen-bound carbons. Thus, although **1a** has a single long ruthenium–carbon length, Ru(2)–C(6), the ring is slipped only by 0.06 Å, which suggests η^6-binding. On the other hand, the ring slippage in **2** is 0.14 Å and the corresponding bond lengths in **2** have two values that are 0.13 Å longer than the average of the other four bond lengths, suggesting η^4-coordination. For comparison, the median ruthenium–carbon bond length in η^6-arene complexes is 2.235 Å.[25] Finally, while the benzoquinone ligand in **2** is planar, the largest out-of-plane deviation being 0.019 Å by the nonbridging oxygen O(1), the nonbridging oxygen in **1a** is bent 0.14 Å out of the plane defined by the remainder of the benzoquinone ligand.

The electronic structures of η^2-O catecholates are most frequently described in terms of the discrete valence tautomers **A–C**, where **A** corresponds to a catecholate complex, $[M^{II}(O_2C_6H_4)^{-II}]$, **B** a semiquinonate complex, $[M^{I}(O_2C_6H_4)^{-I}]$, and **C** a quinone complex, $[M^{0}(O_2C_6H_4)^{0}]$. By far the most sensitive indication of the electronic structure present in a given dioxolene complex is by an X-ray diffraction determination of the carbon–oxygen bond lengths within the metal chelate ring. Typical ranges for complexes assigned to **A**, **B**, and **C** are 1.34–1.37, 1.28–1.31, and 1.23–1.25 Å, respectively.[13] A recent statistical examination of 146 benzoquinone ligands in the Cambridge Structural Database (version 3.10) further supports the use of carbon–oxygen bond lengths as a diagnostic probe of localized electronic structure.[26] This study also concluded that most characterized examples fall into either the semiquinone or catecholate categories, with the few exceptions including $[InBr_2(\eta^2\text{-}O_2C_6H_4)(4Me\text{-}py)_3]$, where the *o*-benzoquinone adopts a structure intermediate between **B** and **C**, and eight cases associated with ruthenium and osmium $[ML_3]$ complexes, which lie between the **A** and **B** limiting forms. For the discussion which follows it is important to bear in mind that all of these results are for non-π-bound η^2-O chelate metallodioxolenes that have the metal coplanar with the quinone.

Two questions which the structures presented in this paper pose are as follows: (1) how is the degree of charge localization affected by π-binding of the quinone to a second metal and (2) what are the electronic consequences for nonplanarity in the metal–quinone ensemble?

In addition to the carbon–oxygen bond length criteria, the π-bonding in **1a** and **2** might allow for an assessment of the redox level of the quinone based on an examination of the metal–carbon bond lengths. In the first approximation, the possibility of η^6-coordination for a catecholate, η^5 for a semiquinone, and η^4 for a quinone (**D–F**) can be

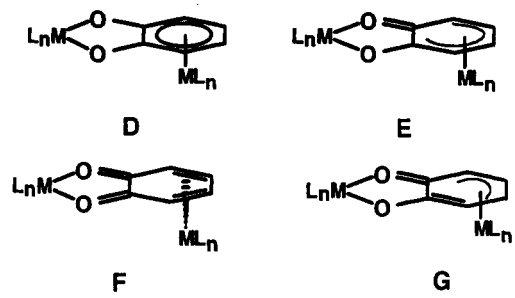

anticipated. In addition, an η^3-semiquinone (**G**), which has been found in $Pd_2\{Pd(DBSQ)_2\}_2$ (DBSQ = 3,5-di-*tert*-butyl-1,2-benzosemiquinone), is also possible and is clearly favored for the later transition metals.[27] Before employing metal–carbon bond lengths or ring slippage to distinguish among **D–F**, it is necessary to consider the general phenomenon of ring slippage in multiring π-arene complexes. Structurally characterized condensed ring aromatics typically have the metal displaced toward the butadiene fragment. That is, the metal–carbon bonds to the junction carbons are usually longer than those to the carbons on the opposite sides of the ring, with the difference in bond lengths often lying in the range 0.1–0.03 Å.[28] This effect has been attributed to the increased stability caused by retention of aromaticity in the non-π-bound ring or to the diminished π-electron density at the ring junction, leading to reduced π-bonding to the metal.[29] A recent structurally characterized complex of benzo[3,4-*c*]-thiophene, $Cr(\eta^6\text{-}C_8H_6S)(CO)_3$, provides a good example of this type of ring slippage; in this case there is a difference of 0.133 Å in the related metal–carbon bond lengths.[30] If the complexes **1a** and **2** are viewed as condensed ring aromatics, then the first explanation suggests that ring slippage would result from an increase in the delocalization of electrons into the five-membered chelate ring. However, as noted by Pierpont, there is no evidence to support such a delocalization model in η^2-O catecholate complexes, and this is unlikely to operate in either **1a** or **2**.[13] On the other hand, *ab initio* calculations for catechol and *o*-benzoquinone indicate reduced electron densities at the oxygen-bearing carbons.[31] Thus, although ring slippage in **D** and **E** is consistent with the valence tautomers shown in each, there is no *a priori* connection between an observed pattern of metal–carbon bond lengths and the redox state of the quinone ligand. Some of the difficulties in interpreting these structural trends are illustrated by the complex $[(Pr^i_2PCH_2)_2Rh\{(\eta^6\text{-}C_6H_4O_2)B(O_2C_6H_4)\}]$. In this case the dicatecholborate anion has a single η^6-π-bound $C_6H_4O_2$ substituent with relatively long carbon–oxygen bond

(25) Orpen, A. G.; Brammer, L.; Allen, F. H.; Kennard, O.; Watson, D. G.; Taylor, R. *J. Chem. Soc., Dalton Trans.* **1989**, S1.
(26) Carugo, O.; Castellani, C. B.; Djinović, K.; Rizzi, M. *J. Chem. Soc., Dalton Trans.* **1992**, 837.
(27) Fox, G. A.; Pierpont, C. G. *Inorg. Chem.* **1992**, *31*, 3718.
(28) (a) Muetterties, E. L.; Bleeke, J. R.; Wucherer, E. J.; Albright, T. A. *Chem. Rev.* **1982**, *82*, 499. (b) Hull, J. W.; Gladfelter, W. L. *Organometallics* **1982**, *1*, 264. (c) Muir, K. W.; Ferguson, G.; Sim, G. A. *J. Chem. Soc. B* **1968**, 467. (d) Cais, M.; Kaftory, M.; Kohn, D. H.; Tatarsky, D. *J. Organomet. Chem.* **1979**, *184*, 103. (e) Hanic, F.; Mills, O. S. *J. Organomet. Chem.* **1968**, *11*, 151.
(29) Huckett, S. C.; Miller, L. L.; Jacobsen, R. A.; Angelici, R. J. *Organometallics* **1988**, *7*, 686.
(30) Selegue, J. P.; Swarat, K. A. *J. Am. Chem. Soc.* **1993**, *115*, 6448.
(31) Kuboyama, A.; Wada, K. *Bull. Chem. Soc. Jpn.* **1965**, *38*, 1709.

lengths, 1.340(8) and 1.346(8) Å, and a ring slipped away from the oxygen-bearing carbons by 0.187 Å.[32] Although this might initially suggest a structure such as **F**, the longest rhodium–carbon bond is to the carbon adjacent to the oxygen-bearing carbons, a structure not in accord with the any of the structures **D–F**. Unfortunately, it is not meaningful to consider the carbon–carbon bond lengths for these ligands due to their inherently high esd's, as well as the general lengthening of these bond lengths in π-arene complexes.

The syntheses of **1a** and **2** illustrate the subtle control that the synthetic conditions have on the outcome of the reaction. It is possible to convert **2** to **1** in high yield by treating it with additional catechol in toluene at reflux (eq 3). This experiment suggests that the $\{Ru(CO)_4\}$-

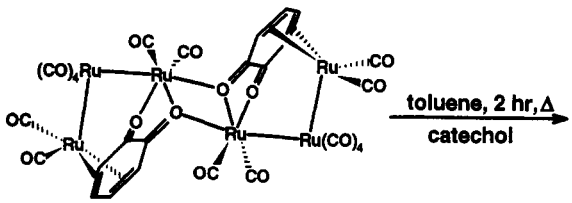

2

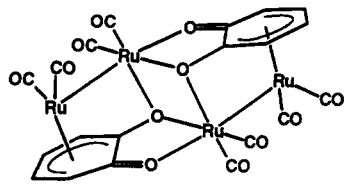

(3)

1a

bridged hexanuclear product **2** is probably an intermediate in the initial oxidative addition of catechol in the preparation of **1**. While it is tempting to speculate on the individual steps in these transformations, the only pertinent mechanistic information concerns the isomer ratio **a**/**b** as a function of the catechol substituents. For catechol this ratio, 18.4, lies preponderantly toward the structure **1a**, whereas for 1,3-di-*tert*-butyl-1,2-benzoquinone, Keister reports an isomer ratio of ~1:2, with a much lower total return (66%).[22] Part of the selectivity in the case of the reaction with catechol is possibly due to the insolubility of **1a**, which may precipitate out of solution as it forms.

The almost complete insolubility of **1a** can be traced to the close intermolecular π-stacking shown in Figure 2. The quinone rings in individual molecules of **1a** stack in an eclipsed fashion to form chains of paired molecules that are symmetry related by an inversion center located at the midpoint between the two parallel rings. The average intermolecular carbon–carbon bond distance, 3.596 Å, is at the lower end of the range (3.61–3.87 Å) found in the Cambridge Structural Database (version 5) for π-stacked tetrachloro-*o*-benzoquinone and phenanthroquinones.[33] Although the tendency for quinone complexes to form intercalation complexes and to π-stack has been noted before,[13] the degree to which this is manifested in **1a**

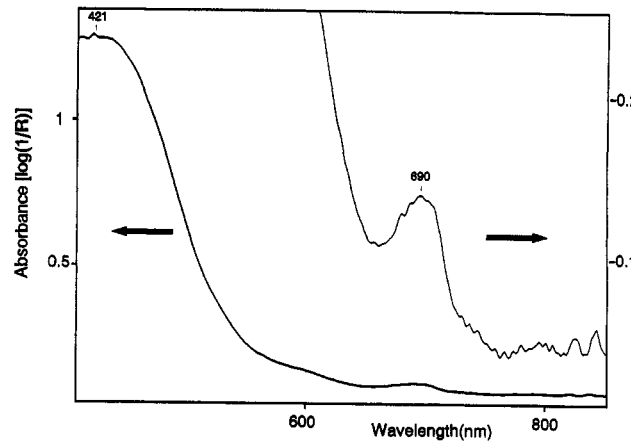

Figure 3. UV–vis diffuse-reflectance spectrum of $[Ru_2(O_2C_6H_4)(CO)_4]_2$ (**1a**).

markedly affects its physical properties. As described in prior communications, the spectroscopic and physical properties of **1a** led us to formulate it as a coordination polymer similar to the carboxylate- and phosphinate-bridged polymers of the $Ru(CO)_2$ fragment.[21a] When bulky substituents such as chlorides or alkyl substituents are present in the catechol, a precipitate does not form. Although these substituents may reduce the strength of the quinone–quinone π-interaction by altering the frontier orbital localization and energies, it is also likely that these substituents would sterically hinder the close approach of the two rings. The diffuse-reflectance electronic spectrum for **1a** has an intense band at 404.6 nm and a weaker band at 690 nm (Figure 3). While the high-energy band is common to both **1a** and **2**, the weak lower energy transition is unique to **1a** and is most likely associated with an intermolecular charge-transfer transition.[34]

Although quinones form a wide range of donor–acceptor complexes with a diverse set of electron donors, self complexes such as **1a**, that is complexes where the same molecule is both acceptor and donor, are relatively unusual for quinones. Donor–acceptor complexes of metallocenes are also uncommon; often other interactions, such as the C–H–N hydrogen bonding in $[CoCp_2][S_3N_3]$,[35] organize the molecules into one-dimensional arrays. The family of η^2-chelate quinonoid complexes is known to form one-dimensional stacks that are typically aligned along a metal–metal axis, especially for square-planar quinonoid complexes of the later transition metals.[36] Clearly the intermolecular π-interactions in **1a** differ from other quinonoid examples. As will be described in the next section, attempts to "dope" the chains with one-electron oxidants such as iodine and nitrosonium tetrafluoroborate lead to other products.

Attempts to prepare a methylated derivative of **1a** from the oxidative addition of 4-methylcatechol to triruthenium dodecacarbonyl have not been successful. Instead of forming an insoluble precipitate similar to **1a**, the products remain in solution. Although we have not attempted to isolate the 4-methyl analogues of **1a,b**, we have prepared the mononuclear derivatives **3c,d** by treating these mixtures with either triphenylphosphine or triphenylarsine

(32) Westcott, S. A.; Taylor, N. J.; Marder, T. B.; Baker, R. T.; Jones, N. J.; Calabrese, J. C. *J. Chem. Soc., Chem. Commun.* **1991**, 304.

(33) For example the quinone ligands in $[Pt(DMSO)_2(\eta^2\text{-}O_2C_6Cl_4)]$[33a] and [Pd(phenanthroquinone)(9,10-dimethylphenanthrene)][33b] form eclipsed stacked dimers with average intermolecular carbon–carbon distances of 3.70 and 3.71 Å, respectively: (a) Khodashova, T. S.; Porai-Koshits, M. A.; Rudii, R. I.; Cherkashina, N. V.; Moiseev, I. I. *Koord. Khim.* **1984**, *10*, 850. (b) Yanovskii, A. I.; Zagorodnikov, V. P.; Struchkov, Yu. T. *Koord. Khim.* **1986**, *12*, 336.

(34) Self donor–acceptor complexes such as **1a** have been reviewed: McGlynn, S. P. *Chem. Rev.* **1958**, *58*, 1113.

(35) Jagg, P. N.; Kelly, P. F.; Rzepa, H. S.; Williams, D. J.; Woolins, J. D.; Wylie, W. *J. Chem. Soc., Chem. Commun.* **1991**, 942.

(36) Chern, S.-S.; Liaw, M.-C.; Peng, S.-M. *J. Chem. Soc., Chem. Commun.* **1993**, 359.

Scheme 1. Reactions of $[Ru_2(\mu_2\text{-}\eta^2\text{:}\eta^6\text{-}O_2C_6H_4)(CO)_4]_2$[a]

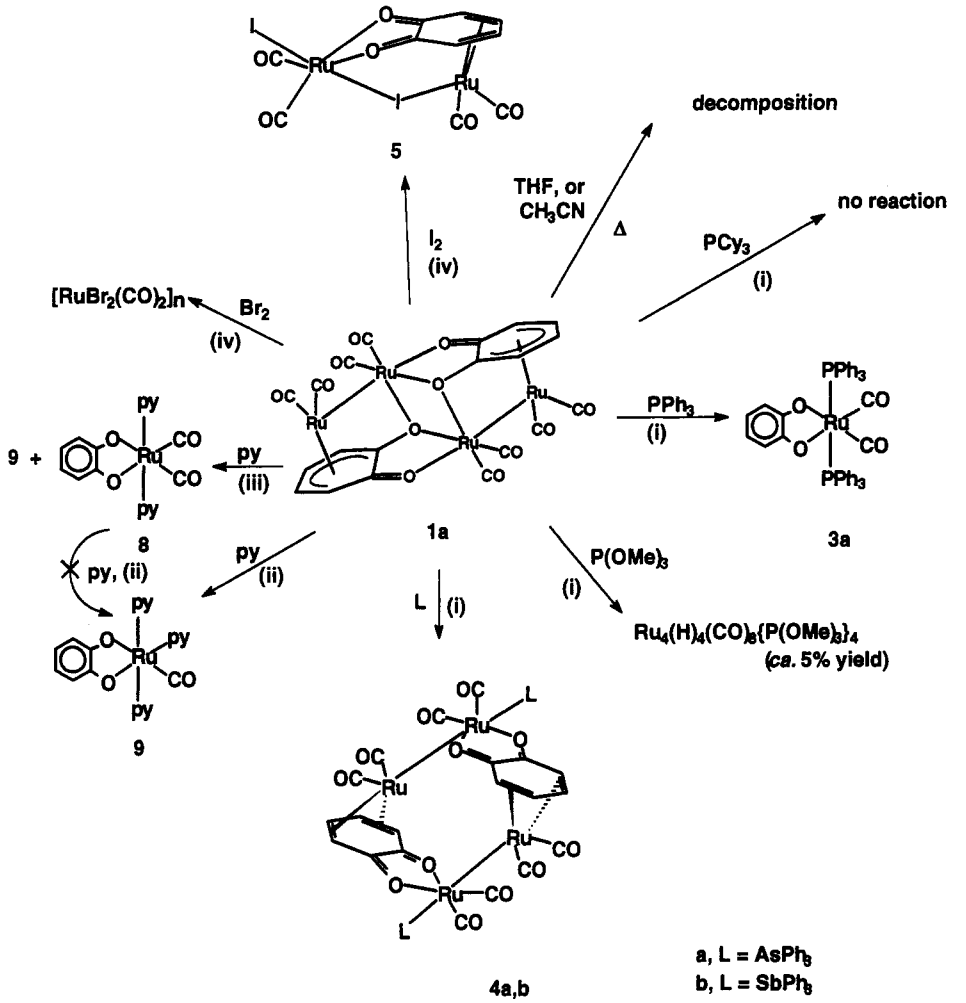

[a] Conditions: (i) ethanol, reflux, 3 h; (ii) neat pyridine, reflux, 2 h; (iii) neat pyridine, 25 °C, 30 h; (iv) CH_2Cl_2, 25 °C, 3 h.

(eq 4). The interpretation of these reactions will be described below.

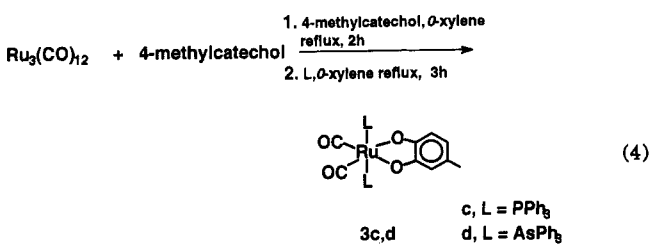

(4)

Reactions of π-Quinone Complexes. The seminal pioneering work of Crooks *et al.* demonstrated that the Ru(I) carboxylate-bridged polymers $[Ru_2(\mu_2\text{-}O_2CR)_2(CO)_4]_n$ are readily cleaved by a wide range of donor ligands such as nitriles, pyridine, phosphites, tertiary phosphines, and tertiary arsines to give the dinuclear complexes $Ru_2(\mu_2\text{-}O_2CR)_2(CO)_4L_2$ in high yields.[24] On the basis of our initial formulation of **1a** as an analogous coordination polymer,[21a] we attempted similar reactions with donor ligands. The results of these experiments are depicted in Scheme 1. Although Lewis bases do indeed react with **1a**, the resulting products vary in nuclearity, oxidation state, and structure.

The contrast in the reactions of tertiary phosphines, arsines, and stibines with **1a** illustrates the variability in the observed products. Although **1a** reacts with excess triphenylphosphine in ethanol at reflux to give the deep red-purple mononuclear complex **3a** in 39% yield, the reaction of **1a** with triphenylarsine and triphenylstibine under the same conditions forms the orange tetranuclear complexes $[Ru_2(\mu_2\text{-}\eta^2\text{:}\eta^4\text{-}O_2C_6H_4)(CO)_4\{EPh_3\}]_2$ (**4a**, E = As; **4b**, E = Sb). Since these ligands have similar cone angles,[37] steric effects alone are unlikely to account for this observed reactivity pattern. However, steric effects are also important, since tris(cyclohexyl)phosphine does not react with **1a** under these conditions. While a bis(triphenylphosphine) analog of **4a,b** is expected to be the first product of the reaction between **1a** and triphenylphosphine, we have not been able to isolate such a species. Attempts to prepare a triphenylphosphine analog of **4a,b** include (i) rigorous control of stoichiometry to 2 equiv of triphenylphosphine/mol of **1a**, (ii) slow addition of a triphenylphosphine solution with a syringe pump over the course of 12 h, and (iii) use of milder conditions, *e.g.* dichloromethane at reflux. In these cases the product is usually a mixture consisting of unreacted **1a** and a very low yield (<10%) of **3a**. Prolonged reflux of **1a** in ethanol or toluene at reflux with additional triphenylarsine for 12 h does not return $Ru(O_2C_6H_4)(CO)_2(AsPh_3)_2$ (**3b**), which can be prepared by another route, described below. Furthermore, **3b** is stable in either ethanol or toluene at reflux, and its absence in the products of the reactions of **1a** with triphenylarsine indicates that it is not formed.

(37) Tolman, C. A. *Chem. Rev.* **1977**, *77*, 313.

When **4a** is treated with a slight excess of triphenylphosphine in ethanol at reflux, a mixture of **3a** and **3b**, that is $Ru(O_2C_6H_4)(CO)_2L_2$ (L = PPh_3, $AsPh_3$), is formed in very low yield. On the basis of the presence of three ν(CO) bands above 2000 cm^{-1} a third mixed isomer, with both triphenylphosphine and triphenylarsine ligands, may also be present in this mixture.

The structure of **4a**, described in detail below, has the triphenylarsine ligand coordinated *trans* to the ruthenium–ruthenium bond. If the metal–metal bond present in **1a** is preserved during the course of the reaction, then ligand addition is accompanied not only by rupture of the oxygen bridges but also by a shift in coordination geometry of the catechol chelate to a site where the oxygens are *trans* to the mutually *cis* carbon monoxide ligands. It is widely recognized that σ-donor ability decreases in the order PR_3 > AsR_3 > SbR_3, and a possible reason for the formation of **3a** instead of the putative triphenylphosphine analog of **4a,b** is that strong σ-donors lead to ruthenium–ruthenium bond heterolysis to give $[Ru^{II}(O_2C_6H_4)(CO)_2(PPh_3)]$ and $[Ru^0(CO)_2]$ fragments. Other strong σ-donors such as pyridine and trimethyl phosphite have a comparable reactivity pattern in that none of the isolable products of these reactions, $[Ru(O_2C_6H_4)(CO)_2(py)_2]$ (**8**), $[Ru(O_2C_6H_4)(CO)(py)_3]$ (**9**), or $[Ru_4H_4(CO)_8\{P(OMe)_3\}_4]$, contain π-benzoquinone ligands. The product distribution of the reaction between **1a** and pyridine is markedly dependent upon the conditions employed. Thus, room-temperature addition of pyridine results in a mixture of the bis(pyridine) complex **8** (62%) and tris(pyridine) complex **9** (38%), but when **1a** is treated with pyridine at reflux, the product is almost solely **9**, with just a trace of **8**, as determined by ^1H NMR. Furthermore, when **8** is treated with pyridine at reflux, **9** is not formed even after 24 h at reflux. This experiment rules out the possibility that **8** is the initial product of this reaction which then partially converts to **9**. Rather, there are clearly two competing pathways by which pyridine, and possibly the other Lewis bases employed in this study, react with **1a**. A surprising implication of these results is that at some point one of the ruthenium dicarbonyl moieties loses carbon monoxide, which allows for the formation of **9**. Since these reactions were performed under ordinary fluorescent lighting, there is no need to invoke adventitious photochemistry to account for these results.

Carbonylation of **1a** at 80 °C in benzene at 60 psi returned **1a** unchanged. For contrast, the carbonylation of $[Ru_2(\mu_2\text{-}O_2CR)_2(CO)_4]_n$ under these conditions results in the formation of a bright yellow solution which contains a species identified as $Ru_2(\mu_2\text{-}O_2CR)_2(CO)_6$ from the IR spectrum.[24] When the pressure of carbon monoxide is removed, this latter complex slowly evolves carbon monoxide to return a precipitate of $[Ru_2(\mu_2\text{-}O_2CR)_2(CO)_4]_n$. Thus, although carbon monoxide can break the interdimer oxygen bridges in these μ_2-carboxylato polymers, it does not do so with **1a**, to give a complex such as $[Ru_4(\mu_2\text{-}O_2C_6H_4)_2(CO)_{10}]$, which would possibly have a structure similar to **4a,b**.

Equation 4 outlines the one-step synthesis of $Ru\{O_2C_6H_3(4\text{-}Me)\}(CO)_2L_2$ (**3c,d**) from triruthenium dodecacarbonyl and 4-methylcatechol. A surprising aspect of this reaction is that both triphenylphosphine and -arsine give mononuclear products with η^2-O-bound catecholate ligands; tetranuclear products such as **4a,b** are never observed. As noted above, a methylated analog of **1a** does not precipitate out of solution during these preparations, and this may be attributed to the split between the two isomers similar to **1a** and **1b** resembling that observed for 3,5-di-*tert*-butylcatechol.[22] Thus, donor ligands may add differently to **1b** than to **1a** and this difference in site of addition may explain the loss of the π-quinone moiety. A related reaction course has been observed for **2**, where addition of triphenylarsine to **2** yields the η^2-O-bound complex **3b** (eq 5). Note that this complex can also be prepared in high yield

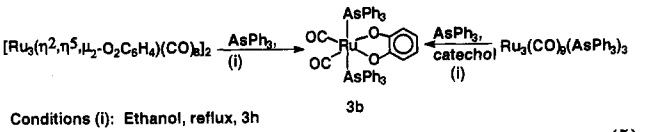

(5)

by treating $Ru_3(CO)_9(AsPh_3)_3$ with catechol and triphenylarsine (eq 5). Surprisingly, **3a** has not been reported, although the tetrachloro analog $Ru(O_2C_6Cl_4)(CO)_2(PPh_3)_2$ was prepared some 20 years ago.[38] A systematic high-yield synthesis of **3a** from $Ru(CO)_2(PPh_3)_3$ and catechol is shown in eq 6. The complexes **3a–d** slowly decompose

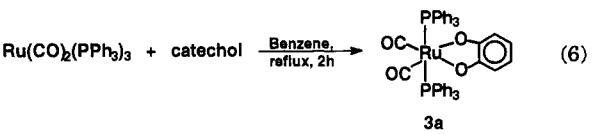

(6)

in halocarbon solvents to give paramagnetic species. Thus, although the electrochemical characterization of **3a–d** is readily performed in dichloromethane, the ^1H and ^{13}C NMR spectral data in Table 2 for these compounds were acquired in C_6D_6. This slow degradation does not require oxygen, and the paramagnetic products have not been identified.

The oxidative cleavage of the ruthenium–ruthenium bond in **1a** with iodine yields $Ru_2(\mu_2\text{-}I)(\eta^2\text{:}\eta^4\text{-}\mu_2\text{-}O_2C_6H_4)(CO)_4I$ (**5**) as an air-stable diruthenium complex bridged by both iodide and quinone. Due to the insolubility of **1a** there is an excess of iodine in solution during the course of the reaction, but there is little appreciable additional reaction between **5** and iodine. On the other hand, the stoichiometric reaction of **1a** with bromine yields a mixture of unreacted **1a** and $[RuBr_2(CO)_2]_n$. Excess bromine yields $[RuBr_2(CO)_2]_n$ in high yield as a bright yellow solid. The fate of the quinone fragment, which is retained in iodine addition product **5**, has not been determined.

The structure of **5**, described below, has both bridging and terminal iodide ligands. Of the three ruthenium–iodide bond lengths in **5**, the terminally bound iodine has the shortest bond length (2.663(1) Å) and the bond between the bridging iodine and the η^2-O-bound ruthenium is the longest (2.773(1) Å). However, the two ruthenium–iodine bond lengths to the bridging iodine are very similar and it is not surprising not only that this bridge is readily opened by weak donors such as acetonitrile but also that both metals are attacked by the incoming ligand. When the reaction of **5** and pyridine is monitored by ^1H NMR, the titer requires *ca.* 5 equiv of pyridine in order for all starting material to be consumed. From this reaction two main products, $Ru_2I_2(O_2C_6H_4)(CO)_4(py)$ (**6**) and $RuI_2(CO)_2(py)_2$ (**7**), can be isolated by column chromatography. The identification of **7** is based on comparison of the IR spectroscopic data (Table 1) to that reported by Hieber

(38) (a) Girgis, A. Y.; Sohn, Y. S.; Balch, A. L. *Inorg. Chem.* **1975**, *14*, 2327. (b) Balch, A. L. *J. Am. Chem. Soc.* **1972**, *95*, 2723.

Scheme 2. Pyridine Addition to $[Ru_2(\mu_2\text{-}\eta^2\text{:}\eta^4\text{-}O_2C_6H_4)(CO)_4]$

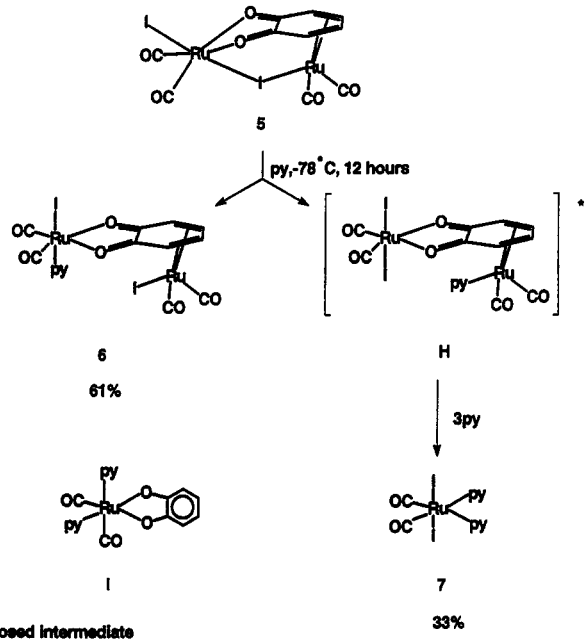

and John.[39] On the basis of the dipole moment of **7** these authors suggest a *trans*-diiodide structure rather than one with *trans*-pyridine ligands. Due the equivalence of the carbonyl and pyridine resonances in the ^1H and ^{13}C NMR spectra of **7** (Table 2) the *all-cis* structure can be ruled out, but the disposition of the mutually *trans* ligands cannot be ascertained.

We propose that the structure of **6** has one iodide ligand per ruthenium and that the pyridine is coordinated *trans* to the terminal iodide on the η^2-O-bound ruthenium. The basis for this proposal is 3-fold: first, the moles of **6** and **7** produced in this reaction amount to the total starting material; second, **7** retains both iodide ligands on one metal; third, this formulation is most consistent with the Raman results described below. Ultimately a single-crystal X-ray diffraction structure for **6** would unambiguously settle this issue; unfortunately, all attempts to obtain suitable crystals result in only thin needles. In addition to **6** and **7** there is a third product in the reaction mixture which decomposes during column chromatography but has ^1H NMR characteristics consistent with **I** in Scheme 2. We attribute the origin of these two products to be due to different sites of attack for the pyridine; cleavage of the μ_2-I bonds in **5** can give either **6** or **H** in Scheme 2. The putative intermediate **H**, which results from coordination to Ru(2), could then coproportionate to give two ruthenium(II) products. That titration of **5** with pyridine requires the addition of 5 equiv can be attributed to the incorporation of three additional pyridine ligands to **H** to give the resulting mononuclear products. The instability of **H** can, in turn, be traced to it being representative of a higher oxidation state manifold for the valence tautomerism:

$$[Ru^{II}(\text{quinone})] \leftrightarrow [Ru^{III}(\text{semiquinone})] \leftrightarrow [Ru^{IV}(\text{catecholate})]$$

The third, albeit unisolated, product in this reaction, **I** in Scheme 2, has two inequivalent pyridine ligands and an asymmetric η^2-O-bound catecholate.[40] The only structure consistent with these results has pairs of mutually *cis* carbon monoxide and mutually *cis* pyridine ligands. Note that **I** is an isomer of **8**, a product of the reaction between **1a** and pyridine, and that **8** is not an observed product (by ^1H NMR) in the reaction between **5** and pyridine.

(39) (a) Hieber, W.; John, P. *Chem. Ber.* **1970**, *103*, 2161. (b) John, P. *Chem. Ber.* **1970**, *103*, 2178.

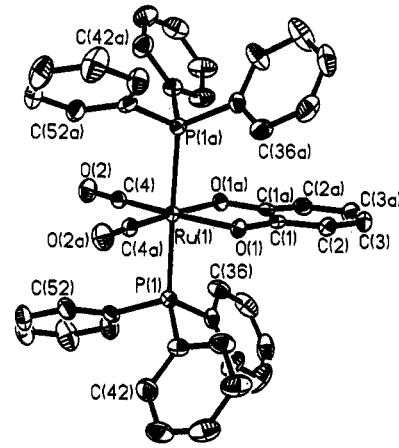

Figure 4. Full molecular structure of $Ru(O_2C_6H_4)(CO)_2(PPh_3)_2$ (**3a**). In this and all subsequent ORTEP projections the hydrogen atoms have been omitted for clarity.

Table 5. Selected Metrical Parameters for $Ru(O_2C_6H_4(CO)_2(PPh_3)_2$ (3a)

Bond Lengths (Å)			
Ru(1)–C(4)	1.877(4)	Ru(1)–O(1)	2.061(2)
Ru(1)–P(1)	2.423(1)	C(1)–C(2)	1.382(5)
C(1)–O(1)	1.347(4)	C(1)–C(1A)	1.403(7)
P(1)–C(31)	1.827(4)	C(2)–C(3)	1.400(6)
P(1)–C(41)	1.827(4)	C(3)–C(3A)	1.369(9)
P(1)–C(51)	1.823(4)		
Bond Angles (deg)			
C(4)–Ru(1)–P(1)	91.5(1)	O(1)–Ru(1)–O(1A)	81.6(1)
C(4)–Ru(1)–O(1)	175.0(1)	C(2)–C(1)–C(1A)	119.4(2)
P(1)–Ru(1)–O(1)	88.9(1)	Ru(1)–O(1)–C(1)	110.6(2)
Ru(1)–C(4)–O(2)	177.8(3)	O(1)–C(1)–C(2)	122.0(3)
P(1)–Ru(1)–C(4A)	89.6(1)	O(1)–C(1)–C(1A)	118.6(2)
O(1)–Ru(1)–C(4A)	93.4(1)	C(4)–Ru(1)–C(4A)	91.6(2)
P(1)–Ru(1)–P(1A)	178.4(1)	C(1)–C(2)–C(3)	120.6(4)
O(1)–Ru(1)–P(1A)	89.9(1)	C(2)–C(3)–C(23A)	119.9(3)

Crystallographic Characterization of 3a, 4a, and 5. In order to have a bench mark to compare the new π-bound *o*-quinone structures, we have structurally characterized the η^2-O-bound catecholate complex **3a** by single-crystal X-ray diffraction. An ORTEP image of **3a** is shown in Figure 4. Selected metrical parameters and atomic positions are collected in Tables 5 and 6, respectively. A crystallographically imposed C_2 axis bisects the ruthenium dicarbonyl and catecholate fragment and relates one half of the molecule to the other. Thus, the single catechol carbon–oxygen bond length C(1)–O(1) (1.347(4) Å) is well within the range ascribed to catecholate ligands[13] but is *ca.* 0.02 Å longer than values found in other structurally characterized ruthenium(II) catecholates.[41] However, unlike most other ruthenium(II) complexes with the general formula $RuX_2(CO)_2(PPh_3)_2$ which are colorless,

(40) In situ ^1H NMR data for the putative species **I** ($CDCl_3$, 400 MHz): δ 8.73 (d, $^3J_{HH}$ = 5.1 Hz, 2, NC_5H_5, C–H_o), 8.34 (d, $^3J_{HH}$ = 5.1, 2, NC_5H_5, C–H_o), 7.75 (t, $^3J_{HH}$ = 5, 1, NC_5H_5, C–H_p), 7.63 (t, $^3J_{HH}$ = 5, 1, NC_5H_5, C–H_p), 7.30 (t, $^3J_{HH}$ = 7, 2, NC_5H_5, C–H_m), 7.20 (t, $^3J_{HH}$ = 6.8, 2, NC_5H_5, C–H_m), 6.68 (d, $^3J_{HH}$ = 7.3, 1, $C_6H_4O_2$, C–H), 6.57 (d, $^3J_{HH}$ = 7.4, 1, $C_6H_4O_2$, C–H), 6.36 (m, 2, $C_6H_4O_2$, C–H).

(41) For comparison, see the structure and discussion in: Bag, N.; Lahiri, G. K.; Basu, P.; Chakravorty, A. *J. Chem. Soc., Dalton Trans.* **1992**, 113.

Table 6. Atomic Coordinates (×10⁵) and Equivalent Isotropic Displacement Coefficients (Å² × 10³) for $Ru(O_2C_6H_4)(CO)_2(PPh_3)_2$ (3a)

	x	y	z	U_{eq}[a]
Ru(1)	0	9 139(4)	25 000	187(1)
C(4)	−3 840(19)	−3 016(35)	18 588(22)	246(12)
O(2)	−6 347(15)	−10 188(28)	14 593(16)	406(10)
P(1)	10 328(5)	9 451(10)	17 410(5)	211(3)
O(1)	3 796(12)	23 620(23)	31 458(14)	223(8)
C(1)	1 885(17)	34 599(33)	28 433(21)	213(11)
C(2)	3 477(21)	45 765(38)	31 922(26)	306(13)
C(3)	1 674(20)	57 030(37)	28 458(28)	380(15)
C(31)	11 549(21)	22 301(34)	10 674(22)	248(12)
C(32)	17 861(26)	27 673(45)	9 670(25)	435(16)
C(33)	18 937(31)	36 556(48)	4 063(29)	582(20)
C(34)	13 594(30)	40 279(46)	−413(26)	489(17)
C(35)	7 283(31)	35 220(47)	506(26)	468(18)
C(36)	6 208(23)	26 087(44)	6 007(23)	358(14)
C(41)	18 173(18)	9 929(40)	23 024(18)	261(11)
C(42)	23 632(23)	2 261(45)	21 470(28)	406(16)
C(43)	29 789(21)	4 083(44)	25 227(38)	509(16)
C(44)	30 394(25)	13 389(52)	30 550(28)	472(18)
C(45)	24 996(25)	20 811(54)	32 346(26)	492(17)
C(46)	18 806(23)	19 138(47)	28 562(26)	410(16)
C(51)	11 126(19)	−4 253(36)	11 305(23)	252(12)
C(52)	11 158(23)	−16 058(40)	14 615(27)	352(15)
C(53)	11 447(27)	−26 529(44)	10 035(32)	463(18)
C(54)	11 607(28)	−25 496(49)	2 138(32)	528(19)
C(55)	11 568(32)	−13 922(51)	−1 176(30)	569(21)
C(56)	11 287(25)	−3 320(44)	3 345(26)	386(16)

[a] Equivalent isotropic U, defined as one-third of the trace of the orthogonalized U_{ij} tensor.

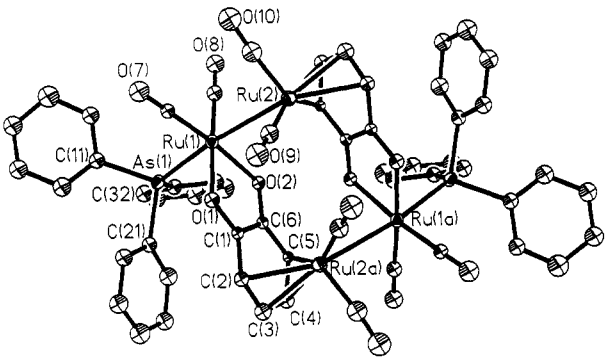

Figure 5. Full molecular view of $[Ru_2(O_2C_6H_4)(CO)_4(AsPh_3)]_2$ (**4a**) from along the crystallographically imposed C_2 symmetry axis.

3a is an intense red-purple (λ_{max} (log ϵ) = 482 nm (3.30)) due to a low-lying charge-transfer band.

The structures of **4a** and **5** were also determined by single-crystal X-ray diffraction to ascertain their exact molecular geometries. The respective ORTEP plots are depicted in Figures 5 and 6, and the important crystallographic results are presented in Tables 7–10.

As described above in the reactions of **1a**, the tetranuclear core of the starting material is retained after addition of triphenylarsine to give **4a**, while in **5** the core is fragmented into two equivalent dinuclear complexes. Although both **4a** and **5** contain π-quinone moieties, there are subtle differences in structure for these two complexes; for example, while the ruthenium dicarbonyl fragment is coplanar with the quinone in **4a**, these two planes intersect with a dihedral angle of 156° in **5**. Molecules of **4a** lie on crystallographic inversion centers that relate the halves of the molecule; the view in Figure 5 is along this axis. Although this symmetry element halved the number of parameters in the refinement of **4a**, and an R value of 4.8% was finally obtained, the amount of data collected

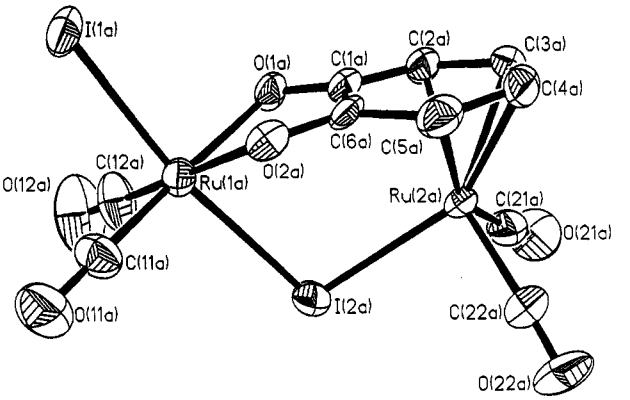

Figure 6. View of molecule A of $Ru_2I_2(CO)_4(O_2C_6H_4)$ (**5**).

Table 7. Selected Metrical Parameters for $[Ru_2(O_2C_6H_4)(CO)_4(AsPh_3)]_2$ (4a)

Bond Lengths (Å)			
Ru(1)–Ru(2)	2.821(2)	C(3)–Ru(2A)	2.235(15)
Ru(1)–As(1)	2.495(2)	C(4)–Ru(2A)	2.259(15)
Ru(1)–C(7)	1.850(16)	C(5)–Ru(2A)	2.356(14)
Ru(1)–C(8)	1.835(16)	C(6)–Ru(2A)	2.583(14)
Ru(1)–O(1)	2.114(10)	O(1)–C(1)	1.303(18)
Ru(1)–O(2)	2.106(10)	O(2)–C(6)	1.302(17)
Ru(2)–C(9)	1.844(17)	C(1)–C(2)	1.427(21)
Ru(2)–C(10)	1.802(19)	C(2)–C(3)	1.379(22)
As(1)–C(11)	1.953(16)	C(3)–C(4)	1.394(22)
As(1)–C(21)	1.947(16)	C(4)–C(5)	1.394(20)
As(1)–C(31)	1.948(15)	C(5)–C(6)	1.429(19)
C(1)–Ru(2A)	2.577(14)	C(1)–C(6)	1.449(20)
C(2)–Ru(2A)	2.321(14)		

Bond Angles (deg)			
Ru(2)–Ru(1)–As(1)	168.1(1)	Ru(1)–Ru(2)–C(3A)	144.1(4)
Ru(2)–Ru(1)–C(7)	96.0(5)	C(9)–Ru(2)–C(3A)	138.0(7)
As(1)–Ru(1)–C(7)	95.4(5)	C(10)–Ru(2)–C(3A)	93.1(7)
Ru(2)–Ru(1)–C(8)	80.9(5)	C(3A)–Ru(2)–C(5A)	62.8(5)
As(1)–Ru(1)–C(8)	95.8(5)	C(3A)–Ru(2)–C(4A)	36.1(6)
C(7)–Ru(1)–C(8)	88.4(7)	Ru(1)–Ru(2)–C(4A)	108.2(4)
Ru(2)–Ru(1)–O(1)	95.7(3)	C(9)–Ru(2)–C(4A)	170.9(6)
As(1)–Ru(1)–O(1)	87.4(3)	C(10)–Ru(2)–C(4A)	98.3(7)
C(7)–Ru(1)–O(1)	92.5(6)	C(4A)–Ru(2)–C(5A)	35.1(5)
C(8)–Ru(1)–O(1)	176.6(6)	Ru(1)–Ru(2)–C(5A)	88.0(3)
Ru(2)–Ru(1)–O(2)	85.0(3)	C(9)–Ru(2)–C(5A)	141.4(6)
As(1)–Ru(1)–O(2)	84.3(3)	C(10)–Ru(2)–C(5A)	127.3(7)
C(7)–Ru(1)–O(2)	171.2(6)	C(9)–Ru(2)–C(10)	88.5(8)
C(8)–Ru(1)–O(2)	100.4(6)	Ru(1)–C(7)–O(7)	178.5(16)
O(1)–Ru(1)–O(2)	78.7(4)	Ru(1)–C(8)–O(8)	177.5(14)
Ru(1)–Ru(2)–C(9)	77.9(5)	Ru(2)–C(9)–O(9)	174.8(15)
Ru(1)–Ru(2)–C(10)	88.5(5)	Ru(2)–C(10)–O(10)	175.2(14)
Ru(1)–Ru(2)–C(2A)	156.9(4)	Ru(1)–O(1)–C(1)	112.1(9)
C(9)–Ru(2)–C(2A)	107.5(6)	Ru(1)–O(2)–C(6)	112.4(9)
C(10)–Ru(2)–C(2A)	113.7(7)	O(1)–C(1)–C(2)	123.8(13)
C(2A)–Ru(2)–C(5A)	73.9(5)	O(1)–C(1)–C(6)	117.8(12)
C(2A)–Ru(2)–C(4A)	64.3(5)	O(2)–C(6)–C(1)	118.3(12)
C(2A)–Ru(2)–C(3A)	35.2(5)	O(2)–C(6)–C(5)	123.1(13)

for this structure was limited by the small size of the crystal used in this study. Consequently, only the ruthenium and arsenic atoms were refined anisotropically. The result is that the esd's for the bonds between the lighter atoms are relatively high, and although the carbon–oxygen bond lengths in the quinone ligand in **4a** (1.295(17) and 1.302(16) Å) are relatively short, these must be considered diagnostic of a trend only. In the unit cell of **5** two independent molecules are present; these differ only slightly from one another in their metrical parameters. Throughout the discussion which follows, an average of the related pairs of metrical data will be employed. In this case the carbon–oxygen bond lengths in the quinone ligand are 1.284(12) and 1.270(11) Å, the shortest determined in this work and well below the range ascribed to semiquinone complexes.[13] Consideration of the ring

Table 8. Atomic Coordinates (×10⁵) and Equivalent Isotropic Displacement Coefficients (Å² × 10³) for $[Ru_2(O_2C_6H_4)(CO)_4(AsPh_3)]_2$ (4a)

	x	y	z	U(eq)[a]
Ru(1)	−11 002(7)	14 002(6)	9 647(9)	207(4)
Ru(2)	4 947(7)	19 088(6)	10 202(10)	238(4)
As(1)	−23 818(8)	7 552(7)	10 774(12)	230(5)
C(7)	−14 723(89)	−19 421(86)	979(96)	222(39)
O(7)	−16 982(67)	22 907(58)	−4 302(78)	438(34)
C(8)	−6 290(96)	−8 926(85)	1 294(102)	285(44)
O(8)	−3 517(68)	−5 805(55)	−4 199(77)	406(33)
C(9)	−1 144(101)	25 853(96)	14 552(111)	342(45)
O(9)	−4 657(70)	30 433(64)	16 874(76)	511(34)
C(10)	3 334(100)	22 340(91)	−462(123)	424(50)
O(10)	2 858(69)	24 335(63)	−7 480(80)	551(39)
O(2)	−7 566(56)	8 880(53)	20 832(60)	206(26)
O(1)	−15 743(59)	20 052(54)	19 452(65)	238(28)
C(11)	−31 529(92)	−7 994(87)	1 188(102)	294(43)
C(12)	−28 164(102)	9 054(82)	−6 997(97)	335(45)
C(13)	−33 049(117)	9 482(98)	−14 175(129)	538(58)
C(14)	−41 643(103)	9 009(92)	−12 869(113)	444(52)
C(15)	−44 973(108)	8 016(86)	−5 016(111)	414(46)
C(16)	−39 658(101)	7 497(86)	2 236(112)	408(46)
C(21)	−30 592(90)	10 072(84)	20 534(102)	256(43)
C(22)	−34 793(92)	15 867(80)	20 351(108)	318(45)
C(23)	−39 368(102)	17 857(86)	27 500(105)	387(45)
C(24)	−39 498(110)	13 823(96)	34 576(113)	466(46)
C(25)	−35 513(92)	8 237(91)	35 965(110)	368(46)
C(26)	−31 039(96)	6 169(88)	27 790(110)	391(50)
C(31)	−22 550(86)	−1 727(73)	12 682(93)	285(43)
C(32)	−28 802(92)	−6 039(75)	10 480(126)	372(41)
C(33)	−28 040(107)	−12 482(88)	12 233(114)	476(55)
C(34)	−20 903(104)	−14 924(102)	15 791(110)	487(53)
C(35)	−14 830(118)	−10 761(95)	17 738(118)	514(56)
C(36)	−15 410(99)	−4 216(88)	15 937(107)	359(46)
C(1)	−14 926(80)	17 524(71)	27 116(91)	163(35)
C(2)	−18 178(82)	20 352(76)	34 786(98)	231(39)
C(3)	−18 047(93)	16 850(78)	42 371(101)	317(46)
C(4)	−13 723(88)	11 080(77)	43 331(98)	258(40)
C(5)	−9 565(75)	8 616(71)	36 195(83)	134(33)
C(6)	−10 421(90)	11 506(68)	27 855(86)	163(33)

[a] Equivalent isotropic U, defined as one-third of the trace of the orthogonalized U_{ij} tensor.

slippage and the metal–carbon bond lengths in **4a** and **5** augment and extend the discussions above for **1a** and **2**. When the average differences in metal–carbon (arene) bond lengths to the two oxygen-bound carbons and those on the opposite side of the ring (Δ = 0.327 Å for **4a** and 0.253 Å for **5**) are calculated, there is clearly substantial ring slippage toward the diene as depicted in the structure **F**. The corresponding slippages away from the centroid are 0.24 Å for **4a** and 0.32 Å for **5**. If the formal oxidation states are assigned to **4a** and **5**, the two distinct ruthenium atoms are best described as Ru(0),Ru(0) in **4a** and either Ru(II),Ru(0) or Ru(I),Ru(I) in **5**, depending upon how the bridging iodide ligand is partitioned. The addition of 2 equiv of iodine to **1a** results in a formal oxidation of the Ru_2(quinone) ensemble by two units. There is a distinct increase in the carbonyl stretching frequencies for **5** as compared to **1a**, consistent with a metal-centered oxidation. In addition, there is a decrease in the carbon–oxygen bond lengths in **5** as compared to **1a**, which lends some support to the formulation of these two complexes as semiquinone in **1a** and quinone in **5**.

Although we have not structurally characterized **6**, there is less ambiguity in assigning oxidation states in this case due to the presence of only a single bridge between the two ruthenium atoms. One description for the bonding in this complex is as a pair of strongly coupled ruthenium(I) centers with $S = 0$, the coupling being mediated by the bridging neutral quinone. Since the NMR spectrum of **6** has sharp signals with little indication of a paramagnetic contact shift, the conclusion is that the metals are strongly coupled. Alternatively, the quinone ligand in **6** can be formulated as a dianion coordinated to two ruthenium(II) centers. Support for this formulation again stems from the carbonyl stretching frequencies, which are well within the range associated with divalent ruthenium complexes.

Table 9. Selected Metrical Parameters for $Ru_2(O_2C_6H_4)(CO)_4I_2$ (5)

	molecule A	molecule B
	Bond Lengths (Å)	
Ru(1)–I(1)	2.663(1)	2.667(1)
Ru(1)–I(2)	2.773(1)	2.775(1)
Ru(1)–O(1)	2.101(5)	2.098(7)
Ru(1)–O(2)	2.102(7)	2.100(6)
Ru(1)–C(11)	1.846(9)	1.853(12)
Ru(1)–C(12)	1.830(12)	1.865(12)
Ru(2)–I(2)	2.718(1)	2.728(1)
Ru(2)–C(21)	1.896(9)	1.912(11)
Ru(2)–C(22)	1.926(11)	1.900(11)
Ru(2)–C(1)	2.452(9)	2.463(8)
Ru(2)–C(2)	2.280(9)	2.307(9)
Ru(2)–C(3)	2.196(12)	2.213(10)
Ru(2)–C(4)	2.231(13)	2.219(10)
Ru(2)–C(5)	2.321(9)	2.307(9)
Ru(2)–C(6)	2.493(8)	2.464(8)
O(1)–C(1)	1.288(12)	1.279(12)
O(2)–C(6)	1.270(9)	1.269(12)
C(1)–C(2)	1.405(11)	1.435(15)
C(1)–C(6)	1.479(11)	1.488(14)
C(2)–C(3)	1.415(16)	1.410(15)
C(3)–C(4)	1.415(14)	1.419(18)
C(4)–C(5)	1.409(13)	1.420(16)
C(5)–C(6)	1.410(14)	1.406(14)
	Bond Angles (deg)	
I(1)–Ru(1)–I(2)	171.5(1)	173.1(1)
I(1)–Ru(1)–O(1)	90.3(2)	91.7(1)
I(2)–Ru(1)–O(1)	82.2(2)	84.4(1)
I(1)–Ru(1)–O(2)	89.4(2)	89.9(1)
I(2)–Ru(1)–O(2)	85.3(2)	83.7(1)
O(1)–Ru(1)–O(2)	78.6(2)	78.3(3)
I(1)–Ru(1)–C(11)	89.4(3)	89.2(3)
I(2)–Ru(1)–C(11)	97.6(3)	94.3(3)
O(1)–Ru(1)–C(11)	173.9(4)	175.7(4)
O(2)–Ru(1)–C(11)	95.3(4)	97.5(4)
I(1)–Ru(1)–C(12)	90.9(4)	90.9(3)
I(2)–Ru(1)–C(12)	94.1(4)	95.2(3)
O(1)–Ru(1)–C(12)	98.4(4)	96.1(4)
O(2)–Ru(1)–C(12)	177.0(4)	174.4(4)
C(11)–Ru(1)–C(12)	87.7(5)	88.1(5)
I(2)–Ru(2)–C(21)	95.8(4)	92.7(3)
I(2)–Ru(2)–C(22)	91.3(4)	94.5(3)
C(21)–Ru(2)–C(22)	90.9(4)	90.0(4)
Ru(2)–C(6)–C(5)	66.4(5)	66.8(5)
C(1)–C(6)–C(5)	117.3(7)	119.3(9)
I(2)–Ru(2)–C(1)	78.9(2)	79.2(2)
I(2)–Ru(2)–C(2)	104.9(3)	106.1(3)
I(2)–Ru(2)–C(3)	141.0(3)	141.7(3)
I(2)–Ru(2)–C(4)	141.1(2)	141.4(3)
I(2)–Ru(2)–C(5)	105.9(3)	105.7(3)
I(2)–Ru(2)–C(6)	79.3(2)	79.5(2)
Ru(1)–I(2)–Ru(2)	98.7(1)	98.2(1)
Ru(1)–O(1)–C(1)	110.0(5)	108.9(6)
Ru(1)–O(2)–C(6)	109.2(5)	111.0(6)
Ru(2)–C(1)–O(1)	127.5(7)	128.9(5)
Ru(2)–C(1)–C(2)	66.1(5)	66.6(5)
O(1)–C(1)–C(2)	123.5(8)	122.8(9)
Ru(2)–C(1)–C(6)	74.1(5)	72.5(4)
O(1)–C(1)–C(6)	116.2(7)	118.8(9)
C(2)–C(1)–C(6)	120.0(9)	118.2(9)
Ru(2)–C(6)–O(2)	128.9(7)	128.4(5)
Ru(2)–C(6)–C(1)	71.1(4)	72.4(4)
O(2)–C(6)–C(1)	118.9(8)	115.5(8)
O(2)–C(6)–C(5)	123.6(7)	124.9(9)

Infrared Spectra. It is well recognized that changes in charge distribution within the quinone–metal ensemble

Table 10. Atomic Coordinates (×10⁴) and Equivalent Isotropic Displacement Coefficients (Å² × 10³) for $Ru_2(O_2C_6H_4)(CO)_4I_2$ (5)

	x	y	z	U(eq)[a]
Ru(1A)	11496(1)	3068(1)	5956(1)	35(1)
Ru(2A)	7325(1)	2299(1)	5501(1)	34(1)
I(1A)	13563(1)	2295(1)	6894(1)	53(1)
I(2A)	9103(1)	3613(1)	5006(1)	45(1)
O(1A)	10376(6)	1419(5)	5389(4)	37(2)
O(2A)	10512(6)	3089(5)	7082(4)	39(2)
C(11A)	12408(11)	4540(8)	6573(7)	49(4)
O(11A)	12970(9)	5457(6)	6969(6)	77(4)
C(12A)	12301(11)	2977(10)	4938(7)	64(5)
O(12A)	12834(10)	2922(10)	4307(6)	115(5)
C(21A)	6130(11)	1699(9)	4214(8)	51(4)
O(21A)	5392(9)	1256(7)	3474(6)	79(4)
C(22A)	6303(10)	3543(9)	5859(8)	55(5)
O(22A)	5761(9)	4277(7)	6068(6)	80(4)
C(1A)	9369(9)	1399(7)	5784(7)	38(3)
C(2A)	8171(9)	614(7)	5324(7)	44(4)
C(3A)	7086(10)	671(8)	5787(8)	52(5)
C(4A)	7164(10)	1558(10)	6688(8)	53(5)
C(5A)	8319(10)	2399(8)	7116(7)	46(4)
C(6A)	9465(8)	2336(7)	6723(6)	31(3)
Ru(1B)	-2011(1)	2605(1)	516(1)	36(1)
Ru(2B)	2159(1)	3271(1)	938(1)	34(1)
I(1B)	-3969(1)	1172(1)	-965(1)	59(1)
I(2B)	245(1)	3944(1)	1951(1)	45(1)
O(1B)	-1048(6)	3023(5)	-484(4)	44(3)
O(2B)	-708(6)	1364(5)	293(4)	39(2)
C(11B)	-2763(10)	2166(9)	1413(7)	50(4)
O(11B)	-3261(9)	1848(7)	1931(6)	77(4)
C(12B)	-3086(11)	3772(9)	640(8)	56(5)
O(12B)	-3728(9)	4481(8)	724(6)	87(5)
C(22B)	3401(11)	3106(8)	2043(8)	48(4)
O(22B)	4178(9)	3007(8)	2688(6)	78(4)
C(21B)	3011(10)	4809(9)	1276(7)	49(4)
O(21B)	3486(9)	5699(7)	1443(6)	75(4)
C(1B)	81(9)	2630(8)	-426(6)	40(3)
C(2B)	1203(10)	3109(9)	-690(6)	51(4)
C(3B)	2439(10)	2665(10)	-588(7)	57(5)
C(4B)	2615(10)	1771(9)	-178(7)	56(4)
C(5B)	1557(9)	1325(8)	149(7)	47(4)
C(6B)	283(9)	1696(7)	5(6)	40(3)
C(7)	-58(14)	931(11)	2636(11)	95(7)
Cl(1)	1354(4)	400(3)	2332(2)	84(2)
Cl(2)	-1279(4)	-89(3)	2677(2)	83(2)

[a] Equivalent isotropic U, defined as one-third of the trace of the orthogonalized U_{ij} tensor.

often result in changes in IR bands for the quinonoid ligand.[42] Moreover, it is often possible to define the oxidation state of the dioxolene ligand by the frequency of the relatively intense C–O stretch.[43] Although for η^2-O-bound chelates these changes are interpreted in terms of the valence tautomers **A–C**, it is expected that π-bonding of the quinonoid fragment will also cause substantial shifts in the IR bands for the quinonoid fragment. Complete infrared data for all relevant complexes are presented in Table 1, and Figure 7 contains the region with strong and highly variable quinone bands for four representative compounds. In Figure 7a,b, which correspond to the initial product **1a** and its iodine addition product, **5**, other metal–ligand and ligand modes are all at higher or lower energies, and the depicted bands are solely due to the quinone ligand. In Figure 7c,d, which corresponds to the pyridine-containing complexes **6** and **8**, respectively, the weak bands marked × are due to the pyridine ligands.

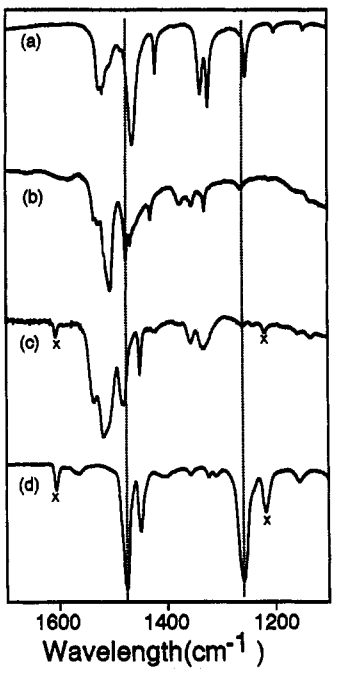

Figure 7. Comparison of representative infrared spectra of the quinonoid bands for (a) $[Ru_2(O_2C_6H_4)(CO)_4]_2$ (**1a**), (b) $Ru_2I_2(CO)_4(O_2C_6H_4)$ (**5**), (c) $Ru_2I_2(py)(CO)_4(O_2C_6H_4)$ (**6**), and (d) $Ru(O_2C_6H_4)(CO)_2(py)_2$ (**8**). Bands due to pyridine ligands in (c) and (d) are marked with an ×, and the dashed lines mark the two intense bands at 1475 and 1258 cm⁻¹ for the catecholate ligand in **8**.

As a representative complex with the well-characterized η^2-O chelate ligand, the spectrum for complex **8** is included in Figure 7d. The two strong bands characteristic of η^2-catecholate coordination, in this instance at 1475 and 1258 cm⁻¹, have been marked with dashed lines. Significantly, the three catecholate complexes **3a**, **8**, and **9** all have identical spectra for this region, apart from strong bands due to the triphenylphosphine ligands in **3a**. On the other hand, the single intense band at 1258 cm⁻¹ in the η^2-catecholate complexes is split into two strong bands for the 4-methylcatecholate complexes **3c,d**. These latter complexes retain the single strong band at *ca.* 1475 cm⁻¹. In analogy to prior work, the band at 1250 cm⁻¹ is assigned to a ν(C–O) mode and the 1475-cm⁻¹ band is attributed to a ring breathing mode. The former band is split upon methylation in **3c,d**, presumably due to the loss of the C_2 symmetry in the ligand.

Lever *et al.* suggest that the ranges for the carbon–oxygen stretching modes vary from 1600 to 1675 cm⁻¹ for η^2-O-bound quinone complexes and from 1400 to 1500 cm⁻¹ for η^2-O-bound semiquinone complexes.[43] Although the spectrum in Figure 7a for **1a** has an intense band attributable to a semiquinone ligand, there are additional bands with medium intensity at 1518 cm⁻¹ for **1a**, at 1505 cm⁻¹ for **5**, and at 1537 and 1518 cm⁻¹ for **6**, which do not conform to these categories. In general, π-coordination of an arene is anticipated to have two major effects on the vibrational spectrum for the arene: population of arene π^* orbitals in the complex is expected to lower the energy of bands associated with the arene, and the attendant vibrational coupling of arene-ring modes with metal modes is anticipated to lower the energy of these modes. Both effects are especially well demonstrated in the π-complexes of the *p*-benzoquinones. π-Back-bonding to the quinone π^* orbital results in a shift in the ν(C—O) bands for the

(42) Haga, M.-A.; Isobe, K.; Boone, S. R.; Pierpont, C. G. *Inorg. Chem.* **1990**, *29*, 3795.
(43) Lever, A. B. P.; Auburn, P. R.; Dodsworth, E. S.; Haga, M.-A.; Liu, W.; Melnik, M.; Nevin, W. A. *J. Am. Chem. Soc.* **1988**, *110*, 8076.

quinone shifted between 14 and 76 cm^{-1} to lower energies.[44] For *p*-benzoquinone Calderazzo reports a shift of *ca.* 100 cm^{-1} for the ν(C=C) bands to lower energies upon η^4-coordination in Mo(η^4-*p*-benzoquinone)$_3$.[45] These bands also have appreciable increases in intensity as well. Similar shifts probably occur in the π-complexes of *o*-benzoquinone described here. The limited infrared data for free *o*-benzoquinones suggests that the ν(C=C) bands should lie between 1600 and 1550 cm^{-1}.[46] However, since all of the species described here contain both η^n-π and η^2-O binding modes, the best comparison for changes in the ring modes is that made in Figure 7, and not with the bands for catechol, *o*-benzoquinone, or *o*-semiquinone. Regardless of the ultimate assignment of the bands for these ligands, infrared spectroscopy is a sensitive diagnostic technique for characterizing the coordination mode of the quinonoid fragment.

Electrochemistry. Prior work by Connelly *et al.* and Balch *et al.* has described in detail the electrochemical behavior of Ru($O_2C_6Cl_4$)(CO)$_2$(PPh$_3$)(L) (L = PPh$_3$, AsPh$_3$, P(OPh)$_3$, pyridine, Cl, Br, I).[38,47] Chemical oxidation of some of these complexes with nitrosonium salts allowed for the isolation of semiquinone complexes as either a hexafluorophosphate salt (L = PPh$_3$) or a neutral complex (L = I). The ESR and IR spectra for these products are consistent with a one-electron ligand oxidation, and the products are formulated as semiquinone complexes of ruthenium(II). Furthermore, because the potentials for the electrochemical oxidation of the non-halide species fall within a relatively narrow range (±150 mV) regardless of the ligand at the metal, the spectroscopic conclusion is supported by the electrochemical results. Our results for the η^2-O-bound catecholate complexes **3a–d**, **8**, and **9** have similar overall trends but also have some surprising differences. The relevant electrochemical data are collected in Table 11, and two representative cyclic voltammograms for these complexes are shown in Figure 8a,b.

The bis(triphenylphosphine) complex **3a** exhibits two reversible (i_{ox}/i_{red} = 1 for scan rates υ = 10–250 mV/s), single-electron, diffusion-controlled redox ($i_{ox}/\upsilon^{1/2}$ constant for υ = 10–250 mV/s) processes with potentials at 791 and −388 mV *vs* the ferrocene/ferrocenium couple. The reversibility of these processes depends on the ligand (L = PPh$_3$, AsPh$_3$, py) and catechol substituent (H, Me). For example, the second oxidation processes for **3b,d**, the two examples which contain triphenylarsine, are only quasi-reversible and have i_{ox}/i_{red} < 0.3 at υ = 50 mV/s. When these results are contrasted with those for the aforementioned tetrachlorocatechol analogues, we find a similar behavior in terms of the reversibility, and a shift in the potential for the process by 640 and 500 mV to less oxidizing potentials for the first and second processes, respectively, in **3a–d**. This shift in half-wave potential parallels that found for the parent and chlorinated quinones,[48] further supporting the assessment that the electron is removed from a ligand-based orbital.

Table 11. Electrochemical Data for New Complexes[a]

η^2-Catecholate Complexes[b]

	Ru($O_2C_6H_3${4-R})(CO)$_2$L$_2$		$E_{1/2}$ vs Fc/Fc$^+$ (Δ, mV)	
	R	L	Ox(II)	Ox(I)
3a	H	PPh$_3$	791 (262)	−388 (262)
3b	H	AsPh$_3$	753 (245)	−431 (241)
8	H	py	860 (153)	−132 (237)
3c	Me	PPh$_3$	676 (170)	−461 (157)
3d	Me	AsPh$_3$	784 (113)	−443 (348)
9	Ru($O_2C_6H_4$)(CO)(py)$_3$		589 (136)	−318 (194)

π-*o*-Benzoquinone Complexes[c]

	$E_{1/2}$ vs Fc/Fc$^+$			
2	1052			−1112
4a	520	256	10*	−712
4b	508	258	33*	−756
5	1132*			−1170
6	964			−1344

[a] All data are in mV and were measured at 22 °C in dichloromethane solutions with 0.1 M tetra-*n*-butylammonium hexafluorophosphate as supporting electrolyte. In each case a platinum-button working electrode, a platinum-wire auxiliary electrode, and a Ag/Ag$^+$ reference electrode were used. [b] All values measured by cyclic voltammetry at 250 mV/s and referenced to the internal ferrocene/ferrocenium couple. [c] All peaks are irreversible except those marked with an asterisk, which are quasi-reversible. The listed values were determined by square wave voltammetry and referenced to an internal ferrocene/ferrocenium couple.

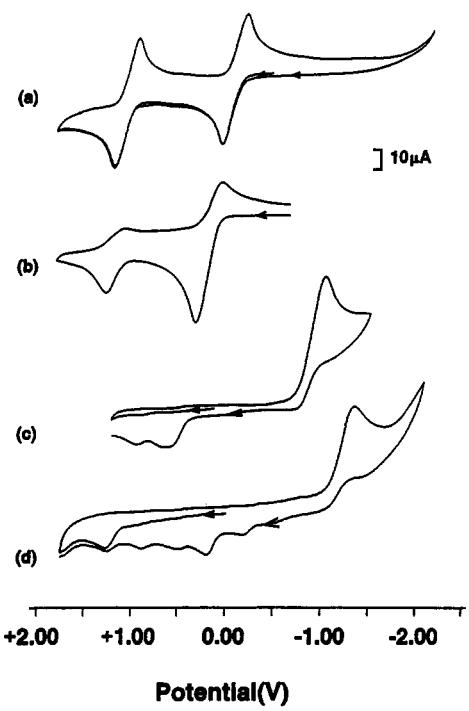

Figure 8. Representative cyclic voltammograms for (a) Ru($O_2C_6H_4$)(CO)$_2$(PPh$_3$)$_2$ (**3a**), (b) Ru($O_2C_6H_4$)(CO)$_2$(py)$_2$ (**8**), (c) Ru$_2$I$_2$(CO)$_4$($O_2C_6H_4$) (**5**), and (d) Ru$_2$I$_2$(py)(CO)$_4$($O_2C_6H_4$) (**6**). All voltammograms were measured at a scan rate of 250 mV/s in dichloromethane solutions with 0.1 M tetra-*n*-butylammonium hexafluorophosphate as a supporting electrolyte.

However, when both axial ligands coordinated to the Ru($O_2C_6H_4$)(CO)$_2$ fragment are pyridines (*cf.* complex **8**), there is a pronounced shift in the half-wave potential for the first process by *ca.* 250 mV to a more oxidizing potential. The corresponding shift in the second process is less (*ca.* 150 mV) but is nevertheless in the same direction. In this instance both processes are only quasi-reversible at even fast scan rates, as is depicted in Figure 8b. When

(44) (a) Cenini, S.; Ugo, R.; La Monica, G. *J. Chem. Soc. A* **1971**, 416. (b) La Monica, G.; Navazio, G.; Sandrini, P.; Cenini, S. *J. Organomet. Chem.* **1981**, *31*, 89. (c) Schrauzer, G. N.; Thyret, H. *Angew. Chem., Int. Ed. Engl.* **1963**, *2*, 478.

(45) Calderzzo, F.; Henzi, R. *J. Organomet. Chem.* **1986**, *10*, 483.

(46) Berger, S.; Rieker, A. In *The Chemistry of Quinoid Compounds*; Patai, S., Ed.; Wiley-Interscience: New York, 1974; pp 163–229.

(47) Connelly, N. G.; Manners, I.; Protheroe, J. R. C.; Whiteley, M. W. *J. Chem. Soc., Dalton Trans.* **1984**, 2713.

(48) Chambers, J. Q. Reference 46, pp 737–793.

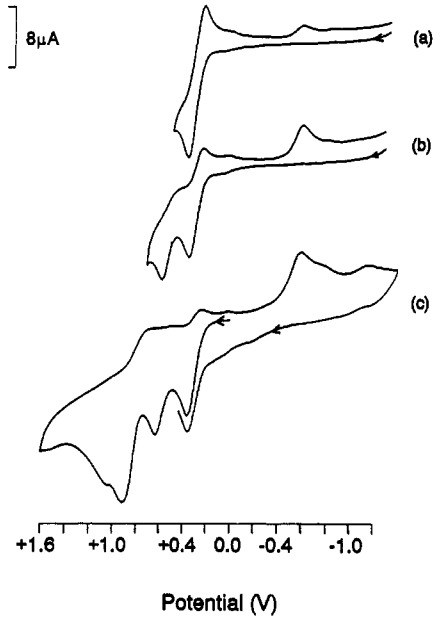

Figure 9. Cyclic voltammograms for $[Ru_2(O_2C_6H_4)(CO)_4(SbPh_3)]_2$ (**4b**) at different switching points after the initial segment (mV): (a) 550; (b) 750; (c) 1600.

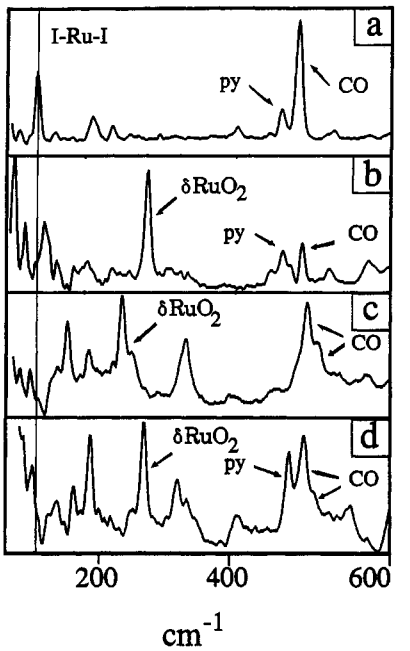

Figure 10. Raman spectra between 100 and 600 cm^{-1} for (a) $RuI_2(CO)_2(py)_2$ (**7**), (b) $Ru(O_2C_6H_4)(CO)_2(py)_2$ (**8**), (c) $Ru_2I_2(CO)_4(O_2C_6H_4)$ (**5**), and (d) $Ru_2I_2(py)(CO)_4(O_2C_6H_4)$ (**6**).

a third pyridine is incorporated into the coordination sphere (complex **9**, $Ru(O_2C_6H_4)(CO)(py)_3$), there is a shift towards more reducing potentials by 150 and 250 mV for the first and second processes, respectively, as compared to **8**. These results once again suggest that the orderings of the orbitals for the metal and quinonoid fragment are very close and sensitive to substitution at either the metal or the quinone.

The electrochemistry of the π-bound quinone complexes, also summarized in Table 11 and in part depicted in Figures 8c,d and 9, is dominated by largely irreversible behavior, which often leads to redox-active products. For example, the cyclic voltammograms for **5** and **6**, shown in Figure 8c,d, are redox inactive up to *ca.* 1 V but after irreversible processes at −1170 and −1344 mV, respectively, result in two new products (with potentials at 38 and 406 mV) in the case of **5**, and at least four new products (with processes at −436, −80, 188, and 584 mV) in the case of **6**, during the return sweep. The irreversible reductions shown in the cyclic voltammograms in Figure 8c,d are unique to these two complexes, and we suggest that they are due to a loss of iodide anion after electron transfer. If this is the case, then loss of either iodine in **6** could give rise to several products after reorganization of the coordination sphere. In **5**, where there are both terminal and bridging iodides present, the smaller number of redox-active products can be attributed to a specific loss of the terminal iodide. The electrochemical behavior of the metal–metal-bonded tetranuclear complexes **4a,b**, as shown in the cyclic voltammograms in Figure 9a–c for the triphenylstibine complex **4b**, is particularly complex. In this case the first oxidation at 33 mV is quasi-reversible ($i_{ox}/i_{red} = 0.42$ at $v = 50$ mV/s) and is followed by two irreversible processes at 258 and 508 mV. These processes in turn lead to new redox-active products with potentials at −472, −865, and −1276 mV. Notably, these processes are absent when the sweep is started at 0 V and run to −1.6 V. The cyclic voltammogram of **2** is complicated by the presence of the catechol solvate in the crystal lattice. Thus, in addition to the two processes listed in Table 11, there are processes at 488 and −1548 mV due to catechol which may overlap with waves due to **2**. Thus, the complexity in the electrochemistry for the metal–metal-bonded species in **4a,b** may also be present but may be disguised by catechol in the case of **2**.

A significant aspect of these results is the alteration π-binding of the *o*-benzoquinone fragment has on the observed electrochemistry of this moiety. As already mentioned, there is an overall loss of reversibility for the π-complexes as compared to the η^2-O-bound chelates. Equally important, however, are the shifts in potentials for processes involved in electron transfer from the quinone ligand. Although we have not determined the nature of the processes involved in the electrochemistry of the π-bound quinonoids, we can conclude that *if* the observed processes in **2** and **3** involve the quinonoid ligand, then *at a minimum* they imply shifts by *ca.* 1400 mV compared to the first process observed in **3a**. This assignment can set a lower limit only. What is more likely the case is that the observed oxidation processes for **2**, **4a,b**, **5**, and **6** are based on the metal or within the π-ligand–metal interaction. Thus, strong π-bonding between the quinonoid fragment and a second metal results in pronounced shifts in potential for the ensemble as a whole. As our understanding of the structures and reactions of the quinoproteins described in the introduction develops, it will be a challenge to ascertain the factors which affect the potential of the metal–quinonoid ensemble and the rate at which it undergoes electron-transfer reactions.

Raman Spectroscopy. In order to establish the exact geometry of pyridine addition to **5**, we have measured the Raman spectra between 600 and 100 cm^{-1} for series of representative complexes. Initially we sought to ascertain the disposition of the iodide ligands **6**: are both on one ruthenium or does each ruthenium have one? If the iodide bridge is cleaved, leaving both iodides on one ruthenium, then they are expected to retain the *trans* configuration in the starting material **5**. Figure 10 contrasts the relevant regions for **7**, **8**, **5**, and **6** in parts a–d, respectively, and a compilation of all Raman data is presented in Table 12. The comparison of the non-catechol-containing mononuclear complex **7**, which has *trans* iodides and *cis*

Table 12. Raman Data for Selected Complexes[a]

compd no.	Ru–I mode	quinone mode	pyridine mode	Ru–CO band
7	137, 161		234, 258, 457	209, 481
8		282, 338	235, 257, 462	204, 486
5	130, 177	250, 262, 335		207, 492, 505
6	133, 189	277, 322	471	207, 487

[a] All data are in cm^{-1} and were measured at 22 °C as crystalline samples sealed in capillary tubes under nitrogen and excited with a Kr^+ laser operating at 647 nm.

pyridines, with the catechol complex 8 allows for an assignment of the modes unique to 7, that is, a strong $\nu(I\text{–}Ru\text{–}I)_{asym}$ band at 137 cm^{-1} and a relatively intense band at 282 cm^{-1} in 8 that we attribute to a catecholate metal–oxygen deformation, $\delta(RuO_2)$. Similar assignments for $\nu(I\text{–}Ru\text{–}I)_{asym}$ and $\delta(RuO_2)$ have been suggested for the Raman-active modes in *cis*- and *trans*-$RuI_2(py)_4$[49] and for $Os(cat)_3$.[50] Common to all four spectra are the bands between 480 and 487 cm^{-1}, which we attribute to the *cis*-carbonyl groups in all four species, although the dinuclear complexes 5 and 6 have two bands in this region which are attributable to the inequivalent environments at the two metal centers.

The intense $\nu(I\text{–}Ru\text{–}I)_{asym}$ band at 137 cm^{-1} for 7 in Figure 10a has been marked with a reference line to facilitate comparison with the other diiodide species. This band is absent in both 5 and 6. In 5 the result of the iodide bridge would be to raise the energy of this mode, and we suggest the intense band at 177 cm^{-1} and the weaker band at 130 cm^{-1} are due to the iodide metal stretching modes.[51] That a single intense band similar to that found in 7 is absent in 6 (*cf.* Figure 10a,d), there being bands at 133 and 189 cm^{-1} that we assign to $\nu(Ru\text{–}I)$, is consistent with our formulation of 6 as having a single iodide on each metal.

The Raman spectra in Figure 10 also illustrate the potential of this technique for determining the total redox state for the metal–quinonoid ensemble. The region between 250 and 450 cm^{-1} is devoid of bands due to pyridine, carbon monoxide, or metal–iodide modes (*cf.* the spectrum of 7 in Figure 10a) but has proven rich in bands due to the quinone ligand. In the catecholate complex 8 this region is dominated by a single intense band, the $\delta(MO_2)$ mode at 282 cm^{-1}, but in the π-bound quinone complex 5 this region contains two bands, the most intense of which is at 250 cm^{-1}. Significantly, the π-complex 6 has both of these features, at 277 and 322 cm^{-1}, but the intense $\delta(MO_2)$ band at 277 cm^{-1} is closer to that found in the catecholate complex 7 rather than to the quinone complex 5. These results suggest that the $\delta(MO_2)$ mode may also be employed as a diagnostic of the valence tautomerization (**A**–**C**) present in a given complex. Furthermore, the lower value for this mode in 5 correlates with it having a longer metal–oxygen bond length. Before this trend can be used, it needs to be tested through an examination of complexes which contain coplanar metal and quinone fragments; although these are likely to be coplanar in 8, in 5 the ruthenium dicarbonyl and quinone fragments are bent. Experiments are underway to determine how the geometry and oxidation level of the metal–quinonoid ensemble influence the energy of the metal–oxygen deformation mode.

Conclusion

A series of new η^2-O chelate and π-quinone complexes of ruthenium have been described in this paper. An early review of the metal–quinonoid complexes observed the dichotomy in binding modes for the family of 1,4-benzoquinones and 1,2-benzoquinones, with the latter preferring chelate formation and the former π-η^4-coordination.[52] In spite of deliberate attempts to prepare π-complexes of 1,2-benzoquinones,[44a,53] this coordination mode has only recently been recognized.[15a] The synthetic approach described in this report utilizes ruthenium clusters which can simultaneously oxidatively add the quinone to one metal center and bind the 1,3-diene-like moiety with a second. Thus, the polynuclear complexes described here are connected not only by the quinone but also by a direct ruthenium–ruthenium bond as in **1a**, by a ruthenium tetracarbonyl fragment as in **2**, by a second $Ru_2(O_2C_6H_4)$ fragment as in **4a,b**, or by an iodide as in **5**. In one instance, compound **6**, the only connection between the two metal centers is the quinone ligand. A simple extension of these results suggests that it might be possible to prepare a mononuclear π-*o*-benzoquinone complex. Clearly, our understanding of the diverse coordination chemistry of the dioxolene fragment is still growing.

Experimental Section

Materials. All starting materials were obtained commercially and used without further purification. Where noted, solvents were dried and degassed by standard techniques but were generally used without further purification. Standard Schlenk and inert-atmosphere-box techniques were used for the preparation of the ^{13}C spectroscopic samples and for the electrochemical experiments. A temperature-monitored Lindberg tube furnace was used in the preparation of **2**. All IR spectra were recorded on a MIDAC FTIR as either a potassium bromide pellet or as a dichloromethane solution between sodium chloride plates. Solution UV–vis data were measured at room temperature on a Hewlett-Packard diode-array spectrometer 8452 with quartz cuvettes. The diffuse-reflectance spectrum for **1a** was acquired on a Perkin-Elmer Lambda-9 spectrometer fitted with a 60-cm integrating sphere and measured against an analytical grade barium sulfate standard. Elemental microanalysis for carbon, hydrogen, and nitrogen was performed by Desert Analytics. Raman spectra were measured on a HR320 spectrograph with a Photometrics CCD9000 liquid nitrogen cooled detector. Laser excitation was made by a Spectraphysics 2025 Kr^+ laser operating at 647 nm.

Preparation of New Compounds. $[Ru_2(\eta^2{:}\eta^6\text{-}\mu_2\text{-}O_2C_6H_4)(CO)_4]_2$ (1a). Triruthenium dodecacarbonyl (90 mg, 1.4×10^{-4} mol) and catechol (320 mg, 2.9×10^{-3} mol) were suspended in 50 mL of degassed *o*-xylene and heated at reflux for 3 h under a nitrogen atmosphere with stirring. An orange solution formed within 30 min, followed by the precipitation of a dense, fine yellow solid. The mixture was cooled to room temperature and then filtered. The resulting yellow crystals were washed thoroughly with methanol (2×10 mL), ethanol (1×10 mL), and finally *n*-hexane to give 81 mg (92% yield) of air-stable product, mp 280–290 °C dec. Anal. Calcd for $C_{20}H_8O_{12}Ru_4$: C, 28.44; H, 0.95. Found: C, 28.53, H; 0.88. UV–vis (diffuse reflectance measured as a dilute NaCl powder): λ_{max} 404.6 (s), 690 nm (w). This microcrystalline product is employed for the preparation of the

(49) Raichart, D. W.; Taube, H. *Inorg. Chem.* **1972**, *11*, 999.
(50) Nielson, A. J.; Griffith, W. P. *J. Chem. Soc., Dalton Trans.* **1978**, 1501.
(51) Nakamoto, K. *Infared and Raman Spectra of Inorganic and Coordination Compounds*, 3rd Ed.; Wiley: New York, 1978; pp 322–324.
(52) Foster, R.; Foreman, M. I. In ref 46, pp 257–335.
(53) Schumann, H.; Arif, A. M.; Richmond, T. G. *Polyhedron* **1990**, *9*, 1677.

derivatives described below. Crystals suitable for single-crystal X-ray diffraction were grown from an unstirred *o*-xylene solution (20 mL) of triruthenium dodecacarbonyl (45 mg) and catechol (292 mg) that was heated at 127 °C for 28 h under nitrogen. The products of both preparations have identical IR and diffuse-reflectance spectra, as well as experimentally measured powder diffraction patterns.

$[Ru_6(\eta^2{:}\eta^4\text{-}\mu_2\text{-}O_2C_6H_4)_2(CO)_{16}]$ (2). Triruthenium dodecacarbonyl (117 mg, 1.8×10^{-4} mol) and catechol (610 mg, 5.5×10^{-3} mol) were placed in a Carius tube and evacuated on a Schlenk line to a pressure of 0.1 mmHg. The tube was then sealed and placed in a preheated tube furnace equilibrated to 140 °C. The triruthenium dodecacarbonyl completely dissolved into the melted catechol, and there was steady evolution of gas over the following 6 h. After 3 days the furnace was cooled to room temperature, the tube was cooled in liquid nitrogen and opened, and the contents were transferred to a sublimation apparatus. Excess catechol and some unreacted triruthenium dodecacarbonyl were then separated by vacuum sublimation onto a water-cooled cold finger at 90 °C and 0.1 mmHg, which leaves behind 122 mg of orange crystals and yellow powder. A crystal suitable for single-crystal X-ray diffraction was picked at this point, and the remainder was recrystallized from dichloromethane/*n*-hexane to yield 0.102 mg (85%) of fine yellow-orange crystals. Anal. Calcd for $C_{28}H_8O_{20}Ru_6 \cdot {}^1/_2C_6H_4(OH)_2$: C, 28.08; H, 0.84. Found: C, 28.42; H, 0.91. UV–vis (in dichloromethane): λ_{max} (log ϵ) 344 (3.86), 446 nm (sh). The presence of the catechol solvate was confirmed by X-ray diffraction, ^1H and ^{13}C NMR, IR, and cyclic voltammetry.

$Ru(O_2C_6H_4)(CO)_2(PPh_3)_2$ (3a). From 1a. $[Ru_2(O_2C_6H_4)(CO)_4]_2$ (**1a**; 96 mg, 2.2×10^{-4} mol) and 230 mg of triphenylphosphine were suspended in 30 mL of ethanol and heated to reflux for 3 h. During this period a deep maroon crystalline solid formed. The suspension was cooled, filtered, washed with ethanol (2×10 mL) and *n*-hexane (2×10 mL), and dried. Recrystallization from dichloromethane/ethanol returned 140 mg (39% yield based on $RuO_2C_6H_4$) of maroon cubes, mp 225–228 °C dec. Anal. Calcd for $C_{44}H_{44}O_4P_2Ru \cdot {}^1/_2CH_2Cl_2$: C, 64.22; H, 4.25. Found: C, 64.10; H, 4.33. The presence of dichloromethane solvate was confirmed by ^1H NMR. UV–vis (in dichloromethane): λ_{max} (log ϵ) 482 nm (3.30). Crystals suitable for single-crystal X-ray diffraction were prepared by recrystallization from a dichloromethane/ethanol solution stored at −42 °C for 3 weeks.

From $Ru(CO)_2(PPh_3)_3$. $Ru(CO)_2(PPh_3)_3$[54] (51 mg, 5.4×10^{-5} mol) and catechol (223 mg, 2.0×10^{-3} mol) were suspended in 50 mL of dry deoxygenated benzene and heated to reflux for 2 h to give a deep maroon solution. This was cooled, diluted with 50 mL of ethanol, and concentrated *in vacuo* to give 33 mg (78% yield) of **3a** as deep maroon crystals that were spectroscopically identical with samples prepared from **1a**.

$Ru(O_2C_6H_4)(CO)_2(AsPh_3)_2$ (3b). From 2. $[Ru_6(O_2C_6H_4)_2(CO)_{16}]_2$ (**2**; 84 mg, 6.6×10^{-5} mol) and 91 mg of triphenylarsine were suspended in 25 mL of ethanol and heated to reflux for 3 h. During this period a deep purple solution developed which upon cooling at −10 °C overnight crystallized as purple blocks. This material was filtered, washed with ethanol (2×10 mL), and recrystallized from dichloromethane/ethanol to return 84 mg (73% yield, based on $RuO_2C_6H_4$) of purple crystals. Anal. Calcd for $C_{44}H_{44}As_2O_4Ru \cdot {}^1/_4CH_2Cl_2$: C, 59.12; H, 3.84. Found: C, 58.92; H, 3.43. The presence of dichloromethane solvate was confirmed by ^1H NMR. UV–vis (in dichloromethane): λ_{max} (log ϵ) 496 nm (3.31).

From $Ru_3(CO)_9(AsPh_3)_3$. $Ru_3(CO)_9(AsPh_3)_3$[55] (60 mg, 4.1×10^{-5} mol), catechol (108 mg), and triphenylarsine (102 mg) were suspended in 20 mL of benzene and heated at reflux for 2 h to give a deep red solution. This was cooled, the benzene was removed *in vacuo*, and the resulting residue was recrystallized from dichloromethane/ethanol to give 80 mg (74% yield) of product that is spectroscopically identical with samples prepared from **2**.

$Ru\{O_2C_6H_3(4\text{-}CH_3)\}(CO)_2(PPh_3)_2$ (3c). Triruthenium dodecacarbonyl (28 mg, 4.4×10^{-5} mol) and 152 mg (1.2×10^{-3} mol) of 4-methylcatechol were suspended in 50 mL of *o*-xylene and heated to reflux for 2 h to give a bright orange solution. Triphenylphosphine (603 mg, 2.3×10^{-3} mol) was then added and the solution heated a further 3 h to give a red solution. The solution was cooled and the *o*-xylene was removed *in vacuo*. The resulting red oil was recrystallized from dichloromethane/ethanol to give 83 mg of product (78% yield) after filtration and successive washes with ethanol (2×10 mL) and *n*-hexane (2×15 mL). Anal. Calcd for $C_{45}H_{36}O_4P_2Ru$: C, 67.24; H, 4.51. Found: C, 67.20; H, 4.41. UV–vis (in dichloromethane): λ_{max} (log ϵ) 494 nm (3.20).

$Ru\{O_2C_6H_3(4\text{-}CH_3)\}(CO)_2(AsPh_3)_2$ (3d). This compound was prepared as described above for **3c** from triruthenium dodecacarbonyl (37.3 mg, 5.8×10^{-5} mol) and 176 mg (1.4×10^{-3} mol) of 4-methylcatechol in 50 mL of *o*-xylene followed by treatment with triphenylarsine (140 mg, 2.3×10^{-3} mol) for 1 h to give a deep purple solution. The solution was cooled and the *o*-xylene was removed *in vacuo*. The resulting red oil was recrystallized from dichloromethane/ethanol to give 94 mg of product (62% yield) after filtration and successive washes with ethanol (2×10 mL) and *n*-hexane (2×15 mL). Anal. Calcd for $C_{45}H_{36}O_4As_2Ru$: C, 59.52; H, 4.18. Found: C, 59.28; H, 4.03. UV–vis (in dichloromethane): λ_{max} (log ϵ) 504 nm (3.13).

$[Ru_2(\eta^2{:}\eta^4\text{-}\mu_2\text{-}O_2C_6H_4)(CO)_4(AsPh_3)]_2$ (4a). $[Ru_2(O_2C_6H_4)(CO)_4]_2$ (**1a**; 30 mg, 3.6×10^{-5} mol) and 61 mg of triphenylarsine were suspended in 20 mL of ethanol and heated to reflux for 1 h. During this period an orange solution formed, followed by precipitation of deep orange crystals. The resulting suspension was cooled, filtered, washed with ethanol (2×10 mL) and hot *n*-hexane (2×10 mL), and dried. Recrystallization from dichloromethane/ethanol returned 50 mg (97% yield) of orange prisms. Anal. Calcd for $C_{56}H_{38}O_{12}As_2Ru_4$: C, 46.16; H, 2.63. Found: C, 46.11; H, 2.53. UV–vis (in dichloromethane): λ_{max} (log ϵ) 467 (4.08), 438 nm (4.05). Crystals suitable for single-crystal X-ray diffraction were prepared by recrystallization from dichloromethane/ethanol.

$[Ru_2(\eta^2{:}\eta^4\text{-}\mu_2\text{-}O_2C_6H_4)(CO)_4(SbPh_3)]_2$ (4b). This compound was prepared as described for **4a** from $[Ru_2(O_2C_6H_4)(CO)_4]_2$ (**1a**; 51 mg, 6.0×10^{-5} mol) and 121 mg of triphenylstibine to give 88 mg of **4b** (86% yield). Anal. Calcd for $C_{56}H_{38}O_{12}Sb_2Ru_4$: C, 43.38; H, 2.47. Found: C, 43.48; H, 2.50. UV–vis (in dichloromethane): λ_{max} (log ϵ) 484 (4.13), 455 nm (4.10).

$Ru_2(\eta^2{:}\eta^4\text{-}\mu_2\text{-}O_2C_6H_4)I_2(CO)_4$ (5). $[Ru_2(O_2C_6H_4)(CO)_4]_2$ (**1a**; 36 mg, 8.5×10^{-5} mol) and 25 mg of iodine (1.2 equiv) were suspended in 10 mL of dichloromethane and stirred for 1 h to give a red-brown solution. *n*-Hexane (10 mL) was added and the mixture concentrated to 2 mL. The red crystals which formed were collected by filtration and washed with *n*-hexane (3×15 mL) to give 49 mg of **5**, in 85% yield. Anal. Calcd for $C_{10}H_4O_6I_2Ru_2$: C, 17.76; H, 0.60. Found: C, 18.14; H, 0.52. UV–vis (in dichloromethane): λ_{max} (log ϵ) 438 nm (3.42). Crystals suitable for single-crystal X-ray diffraction were grown from dichloromethane/*n*-hexane by vapor-phase diffusion.

$Ru_2(\eta^2{:}\eta^4\text{-}\mu_2\text{-}O_2C_6H_4)I_2(CO)_4(py)$ (6). $Ru_2(O_2C_6H_4)I_2(CO)_4$ (**5**; 49 mg, 7.2×10^{-5} mol) was dissolved in 30 mL of dichloromethane and cooled to −78 °C. This solution was then treated with a solution of 23 mg of pyridine (4 equiv) dissolved in 10 mL of benzene, which was added dropwise with a syringe pump over the course of 13 h. Afterward, the solution was warmed to room temperature. The bright yellow-orange solution was then concentrated and chromatographed on silica (2×10 cm column). Elution with 1:1 dichloromethane/hexane gave first a yellow band of $RuI_2(CO)_2(py)_2$ (**7**; 14 mg, 33% yield) and then a yellow-orange band of $Ru_2(O_2C_6H_4)I_2(CO)_4(py)$ (**6**; 33 mg, 61% yield) upon elution with dichloromethane/acetone (10:1). A blue unidentified solid in trace quantities could be isolated by elution of the column with acetone. The complexes **6** and **7** were isolated as crystalline

(54) Cavit, B. E.; Grundy, K. R.; Roper, W. R. *J. Chem. Soc., Chem. Commun.* **1972**, 60.
(55) Bruce, M. I.; Shaw, G.; Stone, F. G. A. *J. Chem. Soc., Dalton Trans.* **1972**, 2094.

Table 13. Data for the X-Ray Diffraction Studies[a]

	1a	3a	4a	5
cryst syst	triclinic	orthorhombic	orthorhombic	triclinic
space group	$P\bar{1}$	*Pbcn*	*Pbcn*	$P\bar{1}$
a (Å)	6.585(2)	19.694(3)	16.412(3)	10.222(2)
b (Å)	8.813(2)	10.770(2)	20.624(3)	12.418(2)
c (Å)	10.416(2)	17.348(2)	15.483(3)	14.621(2)
α (deg)	99.31(3)			107.97(1)
β (deg)	105.65(3)			102.59(1)
γ (deg)	108.92(3)			93.87(1)
V (Å^3)	529.7(2)	3679.6(10)	5240.7(16)	1704.7(5)
Z	1	4	4	4
formula	$C_{20}H_8O_{12}Ru_4$	$C_{44}H_{34}O_4P_2Ru$	$C_{56}H_{38}As_2O_{12}Ru_4$	$C_{10}H_4I_2O_6Ru_2 \cdot {}^1/_2CH_2Cl_2$
fw	844.6	789.7	1457.0	718.55
ρ(calcd) (g cm^{-3})	2.867	1.426	1.847	2.800
collection temp (°C)	23	−100	−100	23
μ (cm^{-1})	0.2867	0.0544	0.2421	0.5503
$R(F_o^2)^a$ (%)	2.09	3.40	4.78	3.26
$R_w(F_o^2)^b$ (%)	2.94	3.36	4.50	4.16
g	0.0008	0.0002	0.0002	0.0006

[a] $R = \sum||F_o| - |F_c||$. [b] $R_w = \sum w(|F_o| - |F_c|)^2$; $w^{-1} = \sigma^2(F) + gF^2$.

solids by recrystallization from dichloromethane/hexane. Characterization data for **6** are as follows. Anal. Calcd for $C_{15}H_9O_6I_2NRu_2$: C, 23.86; H, 1.20; N, 1.85. Found: C, 23.87; H, 1.17; N, 1.80. UV–vis (in dichloromethane): λ_{max} (log ϵ) 362 (3.84), 278 nm (5.01).

Ru(O$_2$C$_6$H$_4$)(CO)$_2$(py)$_2$ (8) and Ru(O$_2$C$_6$H$_4$)(CO)(py)$_3$ (9). [Ru$_2$(O$_2$C$_6$H$_4$)(CO)$_4$]$_2$ (**1a**; 44 mg, 1.04 × 10^{-4} mol) was suspended in 10 mL of neat pyridine and stirred vigorously for 3 days at ambient temperature in an inert-atmosphere box. The resulting yellow-brown solution was dried *in vacuo* and the residue dissolved in 20 mL of dichloromethane and then loaded onto a neutral alumina column (60 mesh Merck Type E, 13 × 1 cm). Dichloromethane was used to elute a trace of brown material, and then 10:1 dichloromethane/acetone was used to elute a light yellow band of Ru(O$_2$C$_6$H$_4$)(CO)$_2$(py)$_2$ (**8**). This fraction was then concentrated to a yellow oil and recrystallized with dichloromethane/heptane to give 27 mg (62% yield) of **8**. A deep orange fraction containing Ru(O$_2$C$_6$H$_4$)(CO)(py)$_3$ (**9**) was then eluted from the column with 5:3 dichloromethane/acetone; concentration followed by recrystallization with dichloromethane/heptane yielded 19 mg (38% yield) of orange needles. Analysis and electronic spectral data for **8** are as follows. Anal. Calcd for $C_{18}H_{14}O_4N_2Ru$: C, 48.12; H, 3.53; N, 7.01. Found: C, 48.15; H, 3.08; N, 7.13. UV–vis (in dichloromethane): λ_{max} (log ϵ) 394 (sh), 310 (3.94), 250 nm (4.23). Analysis and electronic spectral data for **9** are as follows. Anal. Calcd for $C_{22}H_{19}O_3N_3Ru \cdot {}^1/_4CH_2Cl_2$: C, 53.91; H, 3.96; N, 8.48. Found: C, 54.27; H, 4.07; N, 8.15. UV–vis (in dichloromethane): λ_{max} (log ϵ) 428 (3.41), 318 nm (3.99).

X-ray Crystallography. Powder. The X-ray powder pattern of [Ru$_2$(O$_2$C$_6$H$_4$)(CO)$_4$]$_2$ (**1a**) was recorded on a Nonius Guinier camera at 25 °C with Si (a = 5.430 50 Å) as an internal standard and Cu Kα_1 radiation (λ = 1.540 598 Å). The positions of the diffraction lines were measured on a photometer, and the powder pattern was indexed using the program FZON,[56] with the triclinic cell a = 6.584 Å, b = 8.809 Å, c = 10.717 Å, α = 99.31°, β = 105.64°, γ = 110.71°, and $M(20)$ = 16.4 (the figure of merit). From the indexed powder pattern the unit cell parameters were refined by a least-squares procedure using the program CELLKANT.[57] The values obtained in the refinements were a = 6.584(2) Å, b = 8.810(2) Å, c = 10.726(3) Å, α = 99.31(2)°, β = 105.65(2)°, and γ = 108.65(2)° using 52 lines of the pattern.

Single Crystal. Single-crystal X-ray data were collected on a Siemens R3m/V diffractometer equipped with a molybdenum tube (λ(Kα_1) = 0.709 26 Å; λ(Kα_2) = 0.713 54 Å) and a graphite monochromator. Throughout each data collection 3 standard reflections were measured after every 100 reflections collected. In each case the data were corrected for absorption using semiempirical techniques. Structure solution programs used were from the SHELXTL system.[58] The structures were solved by direct methods (**1a**, **2**, **3a**) or Patterson (**4a**, **5**) techniques and refined by full-matrix least-squares techniques. Important X-ray single-crystal parameters are collected in Table 13. Details for each structure follow.

[Ru$_2$(η^2:η^6-μ_2-O$_2$C$_6$H$_4$)(CO)$_4$]$_2$ (1a). Data were collected at 23 °C on a crystal of dimensions 0.38 × 0.06 × 0.18 mm. The compound crystallized in the centrosymmetric triclinic space group $P\bar{1}$, with one molecule in a cell of dimensions a = 6.585(2) Å, b = 8.813(2) Å, c = 10.416(2) Å, α = 99.31(3)°, β = 105.65(3)°, γ = 108.92(3)°, and V = 529.7(2) Å^3. A total of 3097 independent reflections were gathered (R_{int} = 0.019), the octants collected being +h,±k,±l using the Wyckoff scan method. The structure has been refined to conventional R factor values of R = 0.0209 and R_w = 0.0294 on the basis of 2503 observed reflections with $I > 3\sigma(I)$ in the 2θ range 4–60°, giving a data to parameter ratio of 14.0:1. All non-hydrogen atoms were refined anisotropically, while the hydrogen atoms, located in the Fourier map, were refined isotropically. The maximum and minimum residual densities remaining were +0.42 and −0.73 e Å^{-3}, respectively. Selected metrical data and atomic positions are presented in Tables 3 and 4.

[Ru$_3$(η^2:η^4-μ_2-O$_2$C$_6$H$_4$)(CO)$_8$]$_2$·C$_6$H$_4$(OH)$_2$ (2). Data were collected at 23 °C on a crystal of dimensions 0.44 × 0.22 × 0.20 mm. The compound crystallized in the centrosymmetric monoclinic space group $P2_1/n$ with two molecules in a cell of dimensions a = 8.869(1) Å, b = 9.804(2) Å, c = 23.437(5) Å, β = 92.40(1)°, and V = 2036.0(6) Å^3. A total of 4699 independent reflections were gathered (R_{int} = 0.022), the octants collected being −h,+k,±l using the 2θ–θ scan method. The structure has been refined to conventional R factor values of R = 0.0318 and R_w = 0.0477 on the basis of 3153 observed reflections with $I > 3\sigma(I)$ in the 2θ range 4–55°, giving a data to parameter ratio of 9.2:1. All non-hydrogen atoms were refined anisotropically, while the hydrogen atoms, located in the Fourier map, were refined isotropically. The compound crystallizes with half of a catechol solvate per Ru$_3$ asymmetric unit. The catechol molecule is disordered between two orientations related by a 60° rotation of the plane of the molecule which are refined to percent occupancy factors of 32.9 and 17.1%. The carbon atoms in the solvate were refined anisotropically, and the hydrogen atoms were placed in fixed calculated positions (C–H = 0.96 Å). The maximum and minimum residual densities remaining were +0.39 and −0.88 e Å^{-3}, respectively. Selected metrical data and atomic positions are presented in the supplementary material.

(56) Visser, J. W. *J. Appl. Crystallogr.* **1969**, 2, 89.
(57) Ersson, N. O. CELLKANT: Program for Refinement of Cell Parameters; University of Uppsala, Uppsala, Sweden, 1990.
(58) Sheldrick, G. M. SHELXTL Crystallographic System, Version 4.11/V (1990) and Version 4.2/Iris (1991); Siemens Analytical X-ray Instruments, Inc., Madison, WI.

$Ru(\eta^2\text{-}O_2C_6H_4)(CO)_2(PPh_3)_2$ (3a). Data were collected at −100 °C on a crystal of dimensions 0.40 × 0.20 × 0.24 mm. The compound crystallized in the centrosymmetric orthorhombic space group *Pbcn* with four molecules in a cell of dimensions a = 19.694(3) Å, b = 10.770(2) Å, c = 17.348(2) Å, and V = 3679.6(10) Å^3. A total of 4243 independent reflections were gathered, the octants collected being $+h,-k,+l$ using the 2θ–θ scan method. The structure has been refined to conventional R factor values of R = 0.0340 and R_w = 0.0336 on the basis of 2366 observed reflections with $I > 3\sigma(I)$ in the 2θ range 4–55°, giving a data to parameter ratio of 7.9:1. All non-hydrogen atoms were refined anisotropically, while the hydrogen atoms, located in the Fourier map, were refined isotropically. The maximum and minimum residual densities remaining were +0.36 and −0.36 e Å^{-3}, respectively. Selected metrical data and atomic positions are presented in Tables 5 and 6.

$[Ru_2(\eta^2\text{:}\eta^4\text{-}\mu_2\text{-}O_2C_6H_4)(CO)_4(AsPh_3)]_2$ (4a). Data were collected at 23 °C on a crystal of dimensions 0.05 × 0.14 × 0.32 mm. The compound crystallized in the centrosymmetric orthorhombic space group *Pbcn* with four molecules in a cell of dimensions a = 16.412(3) Å, b = 20.624(3) Å, c = 15.483(3) Å, and V = 5240.7(16) Å^3. A total of 4654 independent reflections were gathered, the octants collected being $+h,+k,+l$ using the 2θ–θ scan method. The structure has been refined to conventional R factor values of R = 0.048 and R_w = 0.045 on the basis of 1636 observed reflections with $I > 3\sigma(I)$ in the 2θ range 4–50°, giving a data to parameter ratio of 10.0:1. The Ru and As atoms were refined anisotropically, while all other non-hydrogen atoms were refined isotropically. Hydrogen atoms were placed in fixed calculated positions (C–H = 0.96 Å). The maximum and minimum residual densities remaining were +0.73 and −0.65 e Å^{-3}, respectively. Selected metrical data and atomic positions are presented in Tables 7 and 8.

$Ru_2(\mu_2\text{-}I)(\eta^2\text{:}\eta^4\text{-}\mu_2\text{-}O_2C_6H_4)(CO)_4I\cdot{}^1/_2CH_2Cl_2$ (5). Data were collected at 23 °C on a crystal of dimensions 0.08 × 0.48 × 0.20 mm. The compound crystallized in the centrosymmetric triclinic space group $P\bar{1}$, with four molecules (two independent molecules) in a cell of dimensions a = 10.222(2) Å, b = 12.418(2) Å, c = 14.621(2) Å, α = 107.97(1)°, β = 102.59(1)°, γ = 92.87(1)°, and V = 1704.7(5) Å^3. A total of 5380 independent reflections were gathered, the octants collected being $+h,\pm k,\pm l$ using the 2θ–θ scan method. The structure has been refined to conventional R factor values of R = 0.0326 and R_w = 0.0416 on the basis of 3946 observed reflections with $I > 3\sigma(I)$ in the 2θ range 4–48°, giving a data to parameter ratio of 10.2:1. All non-hydrogen atoms were refined anisotropically, while the hydrogen atoms were placed in fixed calculated sites (C–H = 0.96 Å). The maximum and minimum residual densities remaining were +1.11 and −1.05 e Å^{-3}, respectively. Selected metrical data and atomic positions are presented in Tables 9 and 10.

Electrochemistry. All electrochemistry measurements were performed with a BAS-50W potentiostat in a Vacuum Atmospheres inert-atmosphere box. In each case the cell consisted of a platinum-button working electrode, a platinum-wire auxiliary electrode, and a $Ag/AgNO_3/CH_3CN$ reference electrode with 0.1 M tetra-*n*-butylammonium hexafluorophosphate as backing electrolyte in either dichloromethane or acetonitrile. All reported potential values are referenced to the internal ferrocene/ferrocenium couple.

Acknowledgment. We gratefully acknowledge financial support from the donors of the Petroleum Research Fund (Grant 25141-63), administered by the American Chemical Society, and Professor Jerry Keister for sharing unpublished results with us.

Supplementary Material Available: Tables giving summaries of the X-ray crystallographic results for **1a**, **2**, **3a**, **4a**, and **5**, including additional positional and thermal parameters and bond distances and angles, and a table of observed and calculated powder diffraction lines for **1a** (24 pages). Ordering information is given on any current masthead page.

OM930691Q